

# 1 **Isotopic evidence for biogenic molecular hydrogen production in** 2 **the Atlantic Ocean**

3 S. Walter<sup>1\*</sup>, A. Kock<sup>2</sup>, T. Steinhoff<sup>2</sup>, B. Fiedler<sup>2</sup>, P. Fietzek<sup>2,5</sup>, J. Kaiser<sup>3</sup>, M. Krol<sup>1</sup>, M.  
4 E. Popa<sup>1</sup>, Q. Chen<sup>4</sup>, T. Tanhua<sup>2</sup>, and T. Röckmann<sup>1</sup>

5 [1] Institute for Marine and Atmospheric Research (IMAU), Utrecht University, The  
6 Netherlands

7 \* now Energy research Center of the Netherlands (ECN), Petten, The Netherlands

8 [2] Marine Biogeochemistry, GEOMAR/Helmholtz-Centre for Ocean Research, Kiel,  
9 Germany

10 [3] Centre for Ocean and Atmospheric Sciences, School of Environmental Sciences,  
11 University of East Anglia, Norwich, NR4 7TJ, United Kingdom

12 [4] Department of Atmospheric Sciences, University of Washington, Seattle, Washington,  
13 USA

14 [5] Kongsberg Maritime Contros GmbH, Kiel, Germany

15

16 Correspondence to: S. Walter (s.walter@uu.nl)

17

## 18 **Abstract**

19 Oceans are a net source of molecular hydrogen (H<sub>2</sub>) to the atmosphere. The production of  
20 marine H<sub>2</sub> is assumed to be mainly biological by N<sub>2</sub> fixation, but photochemical pathways are  
21 also discussed. We present measurements of mole fraction and isotopic composition of  
22 dissolved and atmospheric H<sub>2</sub> from the southern and northern Atlantic between 2008 and  
23 2010. In total almost 400 samples were taken during five cruises along a transect between  
24 Punta Arenas (Chile) and Bremerhaven (Germany), as well as at the coast of Mauritania.

25 The isotopic source signatures of dissolved H<sub>2</sub> extracted from surface water are highly  
26 deuterium-depleted and correlate negatively with temperature, showing δD values of (-  
27 629±54) ‰ for water temperatures at (27±3) °C and (-249±88) ‰ below (19±1) °C. The  
28 results for warmer water masses are consistent with biological production of H<sub>2</sub>. This is the

1 first time that marine H<sub>2</sub> excess has been directly attributed to biological production by  
2 isotope measurements. However, the isotope values obtained in the colder water masses  
3 indicate that beside possible biological production a significant different source should be  
4 considered.

5 The atmospheric measurements show distinct differences between both hemispheres as well  
6 as between seasons. Results from the global chemistry transport model TM5 reproduce the  
7 measured H<sub>2</sub> mole fractions and isotopic composition well. The climatological global oceanic  
8 emissions from the GEMS database are in line with our data and previously published flux  
9 calculations. The good agreement between measurements and model results demonstrates that  
10 both the magnitude and the isotopic signature of the main components of the marine H<sub>2</sub> cycle  
11 are in general adequately represented in current atmospheric models despite a proposed  
12 source different from biological production or a substantial underestimation of nitrogen  
13 fixation by several authors.

14

## 15 **1 Introduction**

16 Molecular hydrogen (H<sub>2</sub>) is the second most abundant reduced compound in the atmosphere  
17 after methane (CH<sub>4</sub>). H<sub>2</sub> is not a radiatively active gas itself, but – via its role in atmospheric  
18 chemistry – it indirectly influences the lifetime of the greenhouse gas CH<sub>4</sub> and several air  
19 pollutants (Prather, 2003; Schultz et al., 2003; Tromp et al., 2003; Warwick et al., 2004;  
20 Jacobson, 2008; Feck et al., 2008; Ehhalt and Rohrer, 2009, Popa et al. 2015). The main H<sub>2</sub>  
21 sources are photo-oxidation of CH<sub>4</sub> and non-methane volatile organic compounds (NMVOC)  
22 in the atmosphere and combustion processes at the surface, whereas soil deposition and  
23 oxidation by hydroxyl radicals (HO<sup>•</sup>) are the main sinks. Oceans are a minor but significant  
24 source to the global H<sub>2</sub> budget with a mean estimated contribution of 7 %. However,  
25 estimates of the oceanic contribution range from 1 % to 15 % in different studies, indicating  
26 high uncertainties (Novelli et al., 1999; Hauglustaine and Ehhalt, 2002; Ehhalt and Rohrer,  
27 2009, and references herein, Pieterse et al. 2013).

28 Oceanic H<sub>2</sub> production is assumed to be mainly biological, as a by-product of nitrogen (N<sub>2</sub>)  
29 fixation (e.g. Conrad, 1988; Conrad and Seiler, 1988; Moore et al. 2009, 2014). H<sub>2</sub> is  
30 produced during N<sub>2</sub> fixation in equimolar proportions, but also reused as an energy source.  
31 The H<sub>2</sub> net production rate during N<sub>2</sub> fixation depends on environmental conditions and also  
32 on microbial species (Bothe et al., 1980; 2010; Tamagnini et al., 2007; et al. 2010a). Besides

1 N<sub>2</sub> fixation, abiotic photochemical production from chromophoric dissolved organic matter  
2 (CDOM) and small organic compounds such as acetaldehyde or syringic acid has also been  
3 found to be a source of hydrogen in the oceans (Punshon and Moore, 2008a, and references  
4 therein).

5 Unfortunately, measurements that constrain the temporal and spatial patterns of oceanic H<sub>2</sub>  
6 emissions to the atmosphere are sparse. Vertical profiles display highest concentrations in the  
7 surface layer (up to 3 nmol L<sup>-1</sup>) and a sharp decrease with depth towards undersaturation,  
8 where the reasons for the undersaturation are not fully understood yet (e.g. Herr et al., 1981;  
9 Scranton et al., 1982; Conrad & Seiler 1988). Tropical and subtropical surface waters are  
10 supersaturated up to 10 times or even more with respect to atmospheric H<sub>2</sub> equilibrium  
11 concentrations, and therefore a source of H<sub>2</sub> to the atmosphere. This is in contrast to temperate  
12 and polar surface waters, which are generally undersaturated in H<sub>2</sub> (Scranton et al., 1982; Herr  
13 et al., 1984; Herr, 1984; Conrad and Seiler, 1988; Seiler and Schmidt, 1974; Herr et al., 1981;  
14 Lilley et al. 1982, Punshon et al., 2007, Moore et al. 2014).

15 Additional information to constrain the global H<sub>2</sub> budget and to gain insight into production  
16 pathways comes from the analysis of the H<sub>2</sub> isotopic composition (quantitatively expressed as  
17 isotope delta value,  $\delta D$ , see section 2.2). Different sources produce H<sub>2</sub> with characteristic  $\delta D$   
18 values. Moreover, the kinetic isotope fractionation in the two main removal processes, soil  
19 deposition and reaction with HO<sup>\*</sup>, is different. The combined action of sources and sinks leads  
20 to tropospheric H<sub>2</sub> with a  $\delta D$  of +130 ‰ relative to Vienna Standard Mean Ocean water  
21 (VSMOW), (Gerst and Quay, 2001; Rhee et al., 2006; Rice et al., 2010; Batenburg et al.,  
22 2011). In sharp contrast, surface emissions of H<sub>2</sub> from fossil fuel combustion and biomass  
23 burning have  $\delta D$  values of approximately -200 ‰ and -300 ‰, respectively (Gerst and Quay,  
24 2001; Rahn et al., 2002; Röckmann et al., 2010a; Vollmer et al., 2010). As originally  
25 proposed by Gerst and Quay (2001), isotopic budget calculations require the photochemical  
26 sources of H<sub>2</sub> to be enriched in deuterium, with  $\delta D$  values between +100 ‰ and +200 ‰  
27 (Rahn et al., 2003; Röckmann et al., 2003; Feilberg et al., 2007; Nilsson et al., 2007; Pieterse  
28 et al., 2009; Nilsson et al., 2010; Röckmann et al., 2010b). Biologically produced H<sub>2</sub> has the  
29 most exceptional isotopic composition with  $\delta D$  of approximately -700 ‰ (Walter et al. 2012),  
30 reflecting strong preference of biogenic sources for the lighter isotope <sup>1</sup>H.

31 The aim of the study was I) to determine the  $\delta D$  of dissolved H<sub>2</sub> and gain more information  
32 about possible sources, and II) to get a high-resolution picture of the distribution of

1 atmospheric H<sub>2</sub> along meridional Atlantic transects during different seasons and compare it  
2 with global model results. Samples were taken on four cruises along meridional Atlantic  
3 transects in the southern and northern hemisphere and on one cruise at the coast of  
4 Mauritania. A total of almost 400 atmospheric and 22 ocean surface water samples were  
5 taken, covering two seasons between 2008 and 2010.

## 6 **2 Methods**

### 7 **2.1 Cruise tracks**

8 During four cruises of RV *Polarstern* and one of RV *L'Atalante* between February 2008 and  
9 May 2010, air and seawater samples were collected (see Fig. 1, Table 1). The cruises of RV  
10 *Polarstern* were part of the OCEANET project (Autonomous measuring platforms for the  
11 regulation of substances and energy exchange between ocean and atmosphere, Hanschmann et  
12 al. 2012).

13 They covered both hemispheres, between Punta Arenas (Chile, 53° S / 71° W) and  
14 Bremerhaven (Germany, 53° N / 8° E). South–north transects were carried out in boreal  
15 spring (April / May) and north–south transects in boreal autumn (October / November). The  
16 transects followed similar tracks as the Atlantic Meridional Transect (AMT) programme  
17 (<http://amt-uk.org/>) and crossed a wide range of ecosystems and oceanic regimes, from sub-  
18 polar to tropical and from euphotic shelf seas and upwelling systems to oligotrophic mid-  
19 ocean gyres (Robinson et al. 2009, Longhurst 1998).

20 The RV *L'Atalante* followed a cruise track from Dakar (Senegal) to Mindelo (Cape Verde),  
21 covering a sampling area along the coast of Mauritania and a transect to the Cape Verde  
22 Islands. This area is characterized by strongly differing hydrographical and biological  
23 properties with an intensive seasonal upwelling. Area and cruise track are described in more  
24 detail in Walter et al. (2013) and Kock et al. (2008).

25

### 26 **2.2 Atmospheric air sampling**

27 Discrete atmospheric air samples were taken on–board RV *Polarstern* at the bridge deck,  
28 using 1 L borosilicate glass flasks coated with black shrink-hose (NORMAG), with 2 Kel-F  
29 (PCTFE) O–ring sealed valves. The flasks were pre–conditioned by flushing with N<sub>2</sub> at 50 °C  
30 for at least 12 hours; the N<sub>2</sub> remained in the flask at ambient pressure until the sampling.  
31 During sampling the flasks were flushed for 4 minutes with ambient air at a flow rate of 12 L  
32 min<sup>-1</sup> using Teflon tubes and a membrane pump (KNF VERDER PM22874–86 N86ANDC).

1 The sample air was dried with Drierite® (CaSO<sub>4</sub>). The flasks were finally pressurized to  
2 approximately 1.7 bar, which allows duplicate measurements of the H<sub>2</sub> isotopic composition  
3 of an air sample.

4 Table 1 gives an overview of the sampling scheme for discrete H<sub>2</sub> samples. In total 360  
5 samples were collected, regularly distributed over the transects at 4 to 6 hour intervals. In  
6 2009 the resolution of sampling was enhanced to one sample per two hours and focused on  
7 five sub-sections of the transect, in an attempt to resolve diel variability.

8 Samples were always taken at the downwind side of the ship to exclude a possible  
9 contamination by ship diesel exhaust. One atmospheric sample was taken directly inside the  
10 ship's funnel of RV *Polarstern* to determine the mole fraction and  $\delta D$  of ship diesel exhaust as  
11 a possible contamination source. This first measurements for ship diesel exhaust gave an H<sub>2</sub>  
12 mole fraction of (930.6±3.2) nmol mol<sup>-1</sup> and a  $\delta D$  of (-228.6±5.0) ‰. In the following, we  
13 will use the abbreviation "ppb" = 10<sup>-9</sup> in place of the SI unit "nmol mol<sup>-1</sup>".

14

### 15 **2.3 Headspace sampling from surface waters**

16 In addition to the atmospheric air samples, 16 headspace samples from surface water were  
17 taken during the RV *Polarstern* cruise ANT-XXVI/4 in April / May 2010 and 6 samples  
18 during the RV *L'Atalante* cruise in February 2008. The experimental setup (Fig. 2) was a  
19 prototype, and deployed for the first time to extract headspace air from surface water for  
20 isotopic composition measurements of molecular H<sub>2</sub>. It consists of a glass vessel (10 L) and  
21 an evacuation / headspace sampling unit.

22 The glass vessel was evacuated for at least 24 h before sampling, using a Pfeiffer vacuum  
23 DUO 2.5A pump, with a capacity of 40 L min<sup>-1</sup> (STP: 20° C and 1 bar). Water samples were  
24 taken from 5 m depth (RV *Polarstern* cruises) or 10 m depth (RV *L'Atalante* cruise) using a  
25 24-Niskin-bottle rosette with a volume of 12 L each. Sampling started immediately after  
26 return of the bottle rosette on-board and from a bottle dedicated to the H<sub>2</sub> measurements. The  
27 evacuated glass vessel was connected to the Niskin bottle by Teflon tubing, which was first  
28 rinsed with approximately 1 L surface water. Then, 8.4 L water streamed into the evacuated  
29 flask (Fig. 2), using a drip to enhance the dispersion of the sample water. After connection of  
30 the headspace-sampling unit, the lines were first evacuated and then flushed with a makeup  
31 gas several times. During the RV *L'Atalante* cruise a synthetic air mixture with an H<sub>2</sub> mixing  
32 ratio below threshold was used as makeup gas. The makeup gas used during the RV

1 *Polarstern* cruises was a synthetic air mixture with an H<sub>2</sub> mole fraction of (543.9±0.3) ppb  
2 and a δD of (93.1±0.2) ‰. The mole fraction of the makeup gas was determined by the Max  
3 Planck Institute for Biogeochemistry and is given on the MPI2009 scale (Jordan and  
4 Steinberg, 2011). The glass vessel was pressurized to approximately 1.7 bar absolute with the  
5 makeup gas and the total headspace (added makeup gas plus extracted gas from the water  
6 sample) was then flushed to a pre-evacuated sample flask. The flasks were of the same type  
7 as for the atmospheric sampling: 1 L borosilicate glass flasks (NORMAG), coated with black  
8 shrink-hose to minimize photochemical reactions inside and sealed with 2 Kel-F (PCTFE) O-  
9 ring sealed valves. All flasks were previously conditioned by flushing with N<sub>2</sub> at 50 °C for at  
10 least 12 hours and evacuated for at least 12 hours directly before use. The whole sampling  
11 procedure took around 15 minutes: (4.0±0.5) min flushing surface water to the evacuated  
12 glass vessel, (8.0±1.0) min to connect the glass vessel to the sampling unit and evacuate the  
13 lines, and (3.0±0.5) min to add and pressurize the glass vessel with the makeup gas and take  
14 the headspace sample. The surface water temperature was on average (0.9±0.6) °C higher  
15 than the air temperature. Given that most of the apparatus was at air temperature and that the  
16 headspace will adjust to ambient temperature relatively quickly during equilibration the air  
17 temperature was used for calculations. Since the temperature dependence of H<sub>2</sub> solubility is  
18 less than 0.3 % per K for seawater between 16 °C and 30 °C (as encountered here) and view of  
19 the large H<sub>2</sub> saturations (see below), the error associated with this assumption is negligible.  
20 Flasks were stored in the dark until measurement. At the same location of headspace sampling  
21 also atmospheric samples were taken (Table 4).

22

## 23 **2.4 Measurements**

### 24 **2.4.1 Atmospheric H<sub>2</sub> and δD (H<sub>2</sub>) in discrete samples**

25 The mole fraction and isotopic composition of molecular H<sub>2</sub> was determined using the  
26 experimental setup developed by Rhee et al. (2004) and described in detail in Walter et al.  
27 (2012, 2013) and Batenburg et al. (2011). The D/<sup>1</sup>H molar ratio in a sample,  $R_{\text{sample}}(\text{D}/\text{H})$ , is  
28 quantified as the relative deviation from the D/<sup>1</sup>H molar ratio in a standard,  $R_{\text{standard}}(\text{D}/\text{H})$ , as  
29 isotope delta δD value, and reported in per mill (‰):

30

$$31 \quad \delta D = \frac{R_{\text{sample}}(\text{D}/\text{H})}{R_{\text{standard}}(\text{D}/\text{H})} - 1 \quad (1)$$

32

1 The isotopic standard is Vienna Standard Mean Ocean Water (VSMOW). H<sub>2</sub> mole fractions  
2 are reported as mole fractions in nmol mol<sup>-1</sup>, abbreviated ppb (10<sup>-9</sup>, parts per billion) and  
3 linked to the MPI2009 calibration scale for atmospheric hydrogen (Jordan and Steinberg,  
4 2011). As working standards, atmospheric air from laboratory reference air cylinders and  
5 synthetic air mixtures were used (Walter et al. 2012, 2013, Batenburg et al. 2011); the H<sub>2</sub>  
6 mole fractions of the air in these cylinders were determined by the Max Planck Institute for  
7 Biogeochemistry, Jena, Germany. The atmospheric reference air and the synthetic isotope  
8 reference air were measured daily (atmospheric reference air at least twice) and results were  
9 used for correction of the sample measurements. The uncertainties reported here reflect  
10 random (i.e. repeatability) errors only and do not include possible systematic errors  
11 (Batenburg et al., 2011; Walter et al., 2012, 2013). Samples were measured in random order  
12 and analysed within 3 months (ANT-XXIV/4, ANT-XXV/5, ANT-XXVI/1) up to two years  
13 (ANT-XXVI/4) after sampling. Storage tests indicate that glass flasks equipped with Kel-F  
14 valves are stable for H<sub>2</sub> (Jordan and Steinberg, 2011). The mean measurement repeatability  
15 between the two measurements on the same flask was between ±3.2 ppb (ANT-XXV/5, *n* =  
16 14) and ±6.4 ppb (ANT-XXVI/4, *n* = 108) for the mole fraction and ±3.4 ‰ (ANT-XXVI/4, *n*  
17 = 108) and ±5.0 ‰ (ANT-XXV/5, *n* = 14) for the isotopic composition.

18 H<sub>2</sub> and CO mole fractions were also measured by using a Peak Performer 1 RGA with  
19 synthetic air as a carrier gas, either continuously on-board (ANT-XXVI/4, see section 2.4.2)  
20 or from discrete flasks in the laboratory (ANT-XXV/5 and ANT-XXVI/1). The discrete RGA  
21 measurements were performed from the same glass flasks after measurement of the isotope  
22 system (see above). Due to a remaining slight overpressure in the flasks, an active pumping of  
23 the air into the RGA was not necessary and the flasks were simply connected to the RGA inlet  
24 by Teflon tubing. The remaining pressure was mostly sufficient to perform 8 to 10  
25 measurements. A slight memory effect was observed and thus only the last 5 measurements  
26 were taken into account when stable. Samples with only three or less valid measurements  
27 were not used for evaluation. The standards were the same as those used for the isotope  
28 system. For both cruises (ANT-XXV/5 and ANT-XXVI/1), the mean measurement  
29 repeatability was better than ±0.8 ‰ (H<sub>2</sub>) and ±2 ‰ (CO). A comparison between the H<sub>2</sub> mole  
30 fractions measured with the Peak Performer 1 RGA and the isotopic experimental setup  
31 reveals on average slightly lower RGA values of (7.5±23.8) ppb (see Fig. 3).

32

## 2.4.2 Atmospheric H<sub>2</sub> measured continuously

For the on-board continuous measurements of H<sub>2</sub> mole fractions a Peak Performer 1 RGA was used. The atmospheric air was drawn from the bridge deck to the laboratory in ¼ inch Decabon tubing. The CO mole fraction was also measured in the same measurement and will be reported here for information, but without further discussion.

In alternating order, 10 air samples and 10 aliquots of reference air were measured, using synthetic air as carrier gas. Due to small memory effects, only the last 5 measurements of each were taken into account when the values were stable. The mole fractions of H<sub>2</sub> and CO were calculated by using the mean of the enclosing standard measurements, with an estimated maximal error of ±5 %. For more details see Popa et al. 2014. The mean measurement repeatability for the air samples was ±1.7 % for H<sub>2</sub> and ±3.6 % for CO in ambient air, respectively ±0.8 % (H<sub>2</sub>) and ±0.9 % (CO) for the reference air. Comparing the H<sub>2</sub> mole fractions measured continuously on the RGA with discrete samples measured on the isotope system and collected close in time, we found a mean offset of (−18.8±16.4) ppb for the RGA results.

## 2.4.3 Dissolved H<sub>2</sub> extracted from surface water

The discrete samples of extracted dissolved H<sub>2</sub> were measured as described for the discrete atmospheric samples in section 2.4.1. Details about assumptions and calculations to determine dissolved H<sub>2</sub> concentrations and isotope delta values and quantity symbols are given in detail in the Appendix.

Defining the extraction efficiency  $\eta$  as

$$\eta = \frac{c_h V_h}{c_{w0} V_w} \quad (2)$$

where  $V_h$  and  $V_w$  are the volume of the headspace and the water fraction, and  $c_h$  the concentration of H<sub>2</sub> in the headspace. The initial concentration of H<sub>2</sub> in seawater,  $c_{w0}$ , can be calculated from

$$c_{w0} = \frac{c_h V_h}{\eta V_w} \quad (3)$$

The concentration in the headspace,  $c_h$ , was not measured directly, but can be derived from the measured H<sub>2</sub> mole fraction in the sampling flask. The sampling procedure following gas extraction under vacuum can be broken into three steps (see Methods section):

- 1 1. Expansion of the headspace into the gas transfer system
- 2 2. Addition of makeup gas
- 3 3. Expansion of the headspace / makeup gas mixture into a sample flask

4 As shown in the Appendix, the original concentration of H<sub>2</sub> in seawater (in nmol L<sup>-1</sup>) can be  
5 calculated using the following equation

$$6 \quad c_{w0} = \frac{y_f \left[ \left( 1 + \frac{V_t}{V_h} \right) p_{\text{htm}} - p_h(\text{H}_2\text{O}) \right] - y_m \left[ \left( 1 + \frac{V_t}{V_h} \right) p_{\text{htm}} - p_h \right]}{\eta V_w RT} \quad (4)$$

8  
9 where  $y_f$  is the dry mole fraction of the air in the flask and  $y_m$  the mole fraction of the makeup  
10 gas = (543.9±0.3) ppb.

11 The extraction efficiency,  $\eta$  can be calculated from the following mass balance

$$12 \quad V_w c_{w0} = V_h c_h + \alpha V_w c_h \quad (5)$$

13 Assuming that headspace gas phase and water phase are in equilibrium, the ratio of the H<sub>2</sub>  
14 concentration in water and in the headspace is given by the Ostwald coefficient (where the  
15 concentrations refer to in situ temperature):

$$16 \quad \alpha = \frac{c_w}{c_h} \quad (6)$$

17 This gives for the extraction efficiency as defined in equation (2)

$$18 \quad \eta = \left( 1 + \alpha \frac{V_w}{V_h} \right)^{-1} \quad (7)$$

19 In the present case,  $\alpha = \alpha(\text{H}_2)$  was equal to 0.0163±0.0001, which gives  $\eta = 92.12 (\pm 0.013)\%$   
20 for  $V_w/V_h = 8.4/1.6 = 5.25$ .

21 Two alternative scenarios were considered to derive the  $\delta D$  of the dissolved H<sub>2</sub>, with scenario  
22 1 assuming equilibrium isotopic fractionation between headspace and water, and scenario 2  
23 assuming kinetic isotopic fractionation during extraction from Niskin bottle to glass vessel.

$$24 \quad \text{Scenario 1:} \quad \delta_{w0} = \delta_h + \varepsilon(1 - \eta)(1 + \delta_h) \quad (8)$$

25 The equilibrium isotope fractionation between dissolved phase and gas phase is  $\varepsilon = (37 \pm 1) \text{‰}$   
26 at 20 °C [Knox *et al.*, 1992].

$$27 \quad \text{Scenario 2:} \quad \delta_{w0} = \frac{(1 + \delta_h)\eta}{1 - (1 - \eta)^{1 + \varepsilon_k}} - 1 \approx \delta_h + \varepsilon_k(1 - \eta)(1 + \delta_h) \frac{\ln(1 - \eta)}{\eta} \quad (9)$$

1 The kinetic isotope fractionation during gas evasion is  $\varepsilon_k = (-18 \pm 2) \text{‰}$  at 20 °C [Knox *et al.*,  
2 1992]. The approximation is not used and only shown to illustrate the small difference  
3 between  $\delta_{w0}$  and  $\delta_h$  when  $\eta \approx 1$ .

4 The temperature dependences of  $\varepsilon$  and  $\varepsilon_k$  are unknown and were neglected here.

5 The air saturation equilibrium concentration,  $c_{\text{sat}}(\text{H}_2)$ , was determined using the  
6 parameterization of Wiesenburg and Guinasso (1979). The  $\text{H}_2$  saturation anomaly,  $\Delta(\text{H}_2)$ , was  
7 calculated as the difference between the measured  $\text{H}_2$  concentration,  $c(\text{H}_2)$ , and  $c_{\text{sat}}(\text{H}_2)$ :

$$8 \quad \Delta(\text{H}_2) = c(\text{H}_2) - c_{\text{sat}}(\text{H}_2) \quad (10)$$

9 Meteorological and oceanographic parameters (radiation, air and water temperatures, salinity,  
10 relative humidity) were measured using standard instrumentation and recorded and provided  
11 by the data system of the ships. More information about devices and sensor documentation  
12 can be found on the website of the Alfred Wegener Institute <http://dship.awi.de/>. Backward  
13 trajectories were calculated using the backward “Hybrid Single Particle Lagrangian Integrated  
14 Trajectory” (HYSPLIT, Schlitzer 2012) model of the National Oceanic and Atmospheric  
15 Administration (NOAA, <http://ready.arl.noaa.gov/HYSPLIT.php>).

16

## 17 **2.5 Modeling**

### 18 **2.5.1 TM5 model**

19 We performed simulations of  $\text{H}_2$  mole fractions and isotopic composition with the global  
20 chemistry transport model TM5 (Krol *et al.*, 2005), and compared them with our measurement  
21 data (Fig. 5). The simulation setup was similar to the one of Pieterse *et al.* (2013) and only a  
22 short description is given here. The model version used employs the full hydrogen isotopic  
23 scheme from Pieterse *et al.* (2009) and uses ERA-Interim meteorological data. The chemistry  
24 scheme is based on CBM-4 (Houweling *et al.*, 1998), which has been extended to include the  
25 hydrogen isotopic scheme (that is, for all chemical species that include hydrogen atoms, HH  
26 and HD are treated separately and have different reaction rates). The  $\text{H}_2$  sources and isotopic  
27 signatures are given as input; these and also the  $\text{H}_2$  soil deposition velocities are identical to  
28 Pieterse *et al.* (2013).

29 The model has a relatively coarse spatial resolution of  $6^\circ$  longitude by  $4^\circ$  latitude, and a time  
30 step of 45 minutes. Daily average mole fraction fields are used for comparison to  
31 observations. The model results were interpolated to the time and location of the observations.

32

## 1 **2.5.2 Global oceanic emissions**

2 The climatological global oceanic emissions were calculated using the protocol of Pieterse et  
3 al. (2013), based on the GEMS database and an assumed mean oceanic H<sub>2</sub> source of 5 Tg a<sup>-1</sup>  
4 as given from global budget calculations (see Ehhalt and Rohrer, 2009, and references therein,  
5 Pieterse et al. 2013). The spatial and temporal variability of oceanic H<sub>2</sub> emissions caused by  
6 N<sub>2</sub> fixation are adopted from the spatial and temporal distribution of oceanic CO (Erickson  
7 and Taylor, 1992).

8

## 9 **3 Results and discussion**

### 10 **3.1 Atmospheric H<sub>2</sub> transects**

11 Our data set includes data of two hemispheres and two seasons between 2008 and 2010 (see  
12 Table 2, Fig. 4). The mean mole fraction of H<sub>2</sub> ranged between (532.0±10.7) ppb and  
13 (548.5±6.8) ppb. In spring, the mean values were almost equal between the hemispheres with  
14 approximately 1 to 2 ppb difference, but they differed significantly in autumn. In this season,  
15 the mean values in the northern hemisphere (NH) were approximately 16 ppb or 3 % lower  
16 compared to the southern hemisphere (SH), with a distinct transition between the hemispheres  
17 at around 8° N. In contrast, δD differed significantly between the hemispheres in both  
18 seasons. In the southern hemisphere, absolute δD values were always between 9 and 27 ‰  
19 higher than in the northern hemisphere, and generally remained within a narrow range  
20 between (140.5±21.1) ‰ and (145.4±5.3) ‰. In contrast to the mole fraction, isotope delta  
21 differences between the hemispheres were less pronounced in autumn than in spring. These  
22 two seasonal patterns, in the following defined as “summer signal” and “winter signal”, are  
23 mainly caused by biological processes and tropospheric photochemistry and driven by  
24 variations in the NH. They are in line with previously published data and model results (Rhee  
25 et al. 2006, Price et al. 2007, Rice et al. 2010, Pieterse et al. 2011, 2013, Batenburg et al.  
26 2011, Yver et al. 2011, Yashiro et al. 2011).

27 The “summer signal”, observed in October, is characterized by lower H<sub>2</sub> mole fractions in the  
28 northern hemisphere and a less pronounced difference in δD between the hemispheres.  
29 Deposition by biological activity of microorganisms in the soils is the main sink of H<sub>2</sub>  
30 (Yonemura et al. 2000, Pieterse et al. 2013) and the sink strength in the northern and southern  
31 hemisphere depends on the distribution of landmasses and on season. With approximately 70

1 % of landmasses in the NH and higher microbial activity in the summer, the mole fraction  
2 during this season is lower in the NH than in the SH. Due to the general preference of  
3 organisms for molecules with lighter isotopic composition, the  $\delta D$  values increase during  
4 summer in the NH and the interhemispheric gradient becomes less pronounced.

5 The “winter signal” observed in April is defined by almost equal mole fractions and more  
6 pronounced differences in  $\delta D$  values between the hemispheres. In winter, molecular hydrogen  
7 is accumulating in the NH hemisphere, and the main source is fossil fuel combustion with a  
8 depleted isotopic composition of  $-170\text{‰}$  to  $-270\text{‰}$  (Gerst and Quay, 2001; Rahn et al.,  
9 2002). This leads to nearly equal mole fractions in both hemispheres and a more pronounced  
10  $\delta D$  gradient, with isotopically lighter  $H_2$  in the NH. The contribution of source and sink  
11 processes in the SH to the seasonal patterns is less pronounced than for the NH (Pieterse et al.  
12 2011, 2013). As a result, the  $H_2$  seasonal cycle in the SH is much weaker compared to the  
13 NH. The SH isotopic  $H_2$  signature is caused by mainly emissions and chemical loss with an  
14 isotope delta of approximately  $+190\text{‰}$ , which explains the generally higher  $\delta D$  values. The  
15 Intertropical Convergence Zone (ITCZ) separates the two hemispheres and is clearly visible,  
16 not only in the  $H_2$  distribution, but also in the CO distribution.

17 Simulations of  $H_2$  mole fractions and isotopic composition using the global chemistry  
18 transport model TM5 (Krol et al., 2005) compared with our atmospheric data reveal that the  
19 model simulates the  $H_2$  mole fractions quite well (Fig. 5), with a slight overestimate of up to  
20 20 ppb (which means up to 4 %).

21 The model results are less variable on small spatial scales, due to the low spatial resolution,  
22 and possibly to local influences that are not included in the model (e.g. ocean emissions in the  
23 model are less variable in time and space than they could be in reality). The largest  
24 differences between the modeled and measured  $H_2$  occur between  $30^\circ$  S and the equator. This  
25 seems a systematic feature and could be due to a slight overestimation of sources or  
26 underestimation of sinks by the model. Despite these small differences, the model is  
27 consistent with measured  $H_2$  mole fractions and simulates them well. Large-scale features are  
28 clearly visible, like the sharp gradient around  $10^\circ$  N during cruise ANT-XXVI/1 (Fig. 5, top,  
29 third plot), or the decrease in  $\delta D$  towards northern mid-latitudes (most evident for the cruises  
30 ANT-XXIV/4 and ANT-XXVI/4, first and last plots in Fig. 5, top). A slight overestimate of  
31 the  $H_2$  mole fractions was also noted by Pieterse et al. (2013). This might be explained by an

1 overestimate of photochemical sources in the model, which would influence only the mole  
2 fractions but not the  $\delta D$  values.  
3 The model simulates the isotopic composition of  $H_2$  even better than the mole fractions. The  
4 most important features are the general decrease from south to north, and the sharp gradient  
5 around the equator. As most sources and sinks of  $H_2$  have very different isotopic signatures,  
6 this good comparison indicates that the model represents well both the magnitude and the  
7 isotopic signature of the main components of the  $H_2$  cycle. Similar to Pieterse et al. (2013) we  
8 also observe a slight underestimate of the  $\delta D$  at high southern latitudes, which is possibly due  
9 to underestimating the isotopic composition assumed for  $H_2$  returning from the stratosphere in  
10 the latitude band  $60^\circ S$  to  $90^\circ S$ .  
11

### 12 **3.2 Spatial and temporal high-resolution transects during ANT-XXV/5**

13 In April 2009 the sampling resolution was increased to approximately one sample per two  
14 hours for five selected sections of the transect during ANT-XXV/5 (Fig. 4, Table 3): three in  
15 the southern hemisphere, one crossing the equator and one in the northern hemisphere. These  
16 transects were chosen based on previously published data (Herr et al. 1984, Conrad and  
17 Seiler, 1988) and with the aim to get an indication of small-scale sources or diurnal cycles of  
18 atmospheric  $H_2$  for further investigations.

19 All transects showed neither a diurnal cycle nor a correlation with radiation and a range of  $\delta D$   
20 values within or only slightly outside a  $2\sigma$  range around the mean, except for the one  
21 between  $23.5^\circ S$  to  $15.7^\circ S$  (Fig. 6a). Here the highest  $H_2$  mole fractions of  $(631.9 \pm 3.2)$  ppb,  
22 combined with the lowest  $\delta D$  values of  $(20.9 \pm 5.0)$  ‰, were found around  $16^\circ S$ . Due to the  
23 limited spatial resolution and therefore low number of data points a Keeling plot analysis  
24 (Fig. 6b) of the data between  $15^\circ S$  and  $18^\circ S$  was made with either 5, 7, or 9 data points to  
25 get a reasonable range for the source signature. It reveals a mean source signature of  $-561.5$  in  
26 a range of  $-530$  ‰ to  $-683$  ‰ ( $n = 7 \pm 2$ ,  $R^2 = 0.85 \pm 0.01$ ). The correlation coefficient is a  
27 mean of the three analyses.

28 HYSPLIT trajectories for the samples collected on this transect during the 28 April 2010 and  
29 1 May 2010 ( $21.8^\circ S$  to  $15.7^\circ S$ ) reveal the same origin of air masses coming from the  
30 direction of Antarctica. Oceanographic parameters such as water temperature and salinity are  
31 similar and do not correlate with  $H_2$  mole fractions and  $\delta D$  values. These findings indicate a

1 strong but local source, and the low  $\delta D$  value for the source obtained by the Keeling plot  
2 analysis points to biological production (Walter et al. 2012). Such local and temporal  
3 patchiness of high  $H_2$  mole fractions in surface waters was reported previously in correlation  
4 to high  $N_2$  fixation rates (Moore et al. 2009, 2014). Although reported for other oceanic  
5 regions the  $H_2$  mole fractions and  $\delta D$  values here do neither show a diurnal cycle (Herr et al.  
6 1984) nor they are correlated with radiation indicating photochemical production (Walter et  
7 al. 2013), and most of the values were observed during night. Wilson et al. (2013) recently  
8 showed that  $H_2$  production and uptake rates clearly depends on microbial species, and also on  
9 their individual day–night rhythm, but the contribution of different diazotrophs to the marine  
10  $H_2$  cycle is unknown (e.g. Bothe et al., 2010; Schütz et al., 2004; Wilson et al., 2010a and  
11 2010b; Punshon and Moore, 2008b; Scranton 1983, Moore et al., 2009).

12 Around  $21.2^\circ$  S one single sample with a low mole fraction of  $(393.9 \pm 3.2)$  ppb in  
13 combination with a high  $\delta D$  of  $(322.45 \pm 5)$  ‰ value was observed. As mentioned before  
14 HYSPLIT models reveal the same origin of air masses on this transect, thus this sample  
15 indicates probably a local sink. However, this interpretation depends on only one single  
16 measurement point and although neither instrumental parameters indicated an outlier nor  
17 meteorological or oceanographical parameters differed from other samples, we cannot  
18 exclude an artefact due to sampling, storage, or analyses. A simple Rayleigh fractionation  
19 model reveals a fractionation factor of  $\alpha = 0.646 \pm 0.002$ , which is close to the value of  
20 oxidation by  $HO\cdot$  ( $\alpha = 0.58 \pm 0.07$ , Batenburg et al. 2011). An estimate of the  $\delta D$  value by  
21 using an  $HO\cdot$  oxidation fractionation factor would lead to an increase by 125 ‰ or 149 ‰,  
22 respectively. The observed increase of  $\delta D$  seems reasonable when assuming oxidation by  
23  $HO\cdot$ , but with respect to the  $HO\cdot$  mole fraction and the slow reaction rate of  $H_2 + HO\cdot$  it is  
24 questionable whether the  $H_2$  decrease here can be explained by this.

### 25 **3.3 Dissolved $H_2$**

26 A new method has been presented to extract  $H_2$  from surface waters for isotopic  
27 determination. Before discussing the measurement results, we will give an overview of the  
28 possible main errors and their effects. To show the effect of the errors on the measurements,  
29 we will present error factors, thus how much the final data differ by shifting the respective  
30 parameter by 1 % and also the absolute assumed error.

1 For the extraction method several error sources could be identified: the determination of  
2 pressure, especially in the sampling vessel before adding the make-up gas and during  
3 extraction, the temperature of air and water, respectively the difference between them when  
4 the sample is extracted from the headspace, and the volume of the set-up and the sample. The  
5 determination of pressure in the sampling vessel would be one issue of further improvement,  
6 because the error caused by pressure deviations for the total pressure after adding the make-  
7 up gas is about a factor of 0.7 for concentrations and 0.2 for the isotopic values. The error  
8 based on temperature of air, water and sample is negligible due to high-precision  
9 measurements and the short handling time between water sampling and headspace extraction.  
10 The error for the volume parameter for the set-up is negligible due to the high volume, the  
11 precise determination of the glass vessel volume by weighing, and the calculation of the  
12 tubing volume. The main error source is the water volume of the sample, which counts by a  
13 factor of 5.9 for the concentration, but with negligible effect on the isotopic values. Although  
14 the relative error factor is quite high the absolute value is assumed to be around 0.5% due to  
15 the sample size, which has also been weighed at the home lab. The H<sub>2</sub> measurement  
16 procedure is the same as for atmospheric samples and possible errors are described in the  
17 respective sessions or related literature. However, the error caused by the determination of the  
18 dry mole fraction itself seems to have the main input by a factor of 5.3 for concentration and  
19 4.6 for the isotopic values of dissolved H<sub>2</sub>. Errors of the determination of the isotopic value  
20 are much less significant and count by a factor of 0.2.

21 Taking measurement and handling errors during the extraction as well as errors in the  
22 determination of the dry mole fraction into account, we assume a robust overall uncertainty of  
23  $\pm 6.9 \%$  for the dissolved H<sub>2</sub> mole fractions and  $\pm 4.7 \%$  for the isotopic values by calculating  
24 the root of the sum of the squared uncertainties.

25 As shown in Table 4 we also tested the effect of equilibrium isotopic fractionation and kinetic  
26 isotopic fractionation. The effect is less than 0.2%.

27 Therefore, recommendations for the extraction method are to additionally measure parameters  
28 such as the initial pressure in the glass vessel and to ensure a precise determination of the  
29 sample volume. Besides this we recommend high-precision IRMS measurements and to  
30 consider multiple sampling for better statistics on the data.

31

### 32 **3.3.1 H<sub>2</sub> concentration**

1 In total 16 headspace samples were taken during the RV *Polarstern* cruise in April / May  
2 2010 along the transect 32.53° W / 18.79° S to 13.00° W / 36.54° N and 6 samples during the  
3 RV *L'Atalante* cruise in February 2008 between 23.00 – 17.93° W to 16.9 – 19.2° N to  
4 analyse the H<sub>2</sub> mole fraction and the isotopic composition (see Table 4).

5 Although our setup was a prototype with possibilities for improvement, the mole fractions are  
6 in line with previously published data. The H<sub>2</sub> excess,  $\Delta(\text{H}_2)$ , exceeds 5 nmol L<sup>-1</sup>, the  
7 saturation differ from close to equilibrium to 15-fold supersaturation. Highest supersaturation  
8 was found in the southern hemisphere between 16° S and 11° S and in the northern  
9 hemisphere around the Cape Verde islands and the coast of Mauritania (Fig. 7a, Table 4).

10 Herr et al. (1984) reported patchy enhanced H<sub>2</sub> concentrations in the surface water with up to  
11 5-fold supersaturation in the subtropical south Atlantic (18 – 31° W and 29 – 42° W). This is  
12 comparable to what Conrad and Seiler (1988) found in the Southern Atlantic, on a similar  
13 cruise track as the RV *Polarstern*. Around the equator they measured H<sub>2</sub> surface water  
14 concentrations up to 12-fold supersaturation. In the Southern Pacific, Moore et al. (2009)  
15 combined H<sub>2</sub> surface water measurements with N<sub>2</sub> fixation measurements. They reported a  
16 strong correlation between these parameters, a patchy distribution and a steep maximum of H<sub>2</sub>  
17 concentrations up to 12.6 nmol L<sup>-1</sup> around 14° S.

18 The recently published data by Moore et al. (2014) show similar patterns across the Atlantic  
19 as we found, with highest values around the southern and northern subtropics. However, our  
20 saturations are lower than the ones given by them, especially in the northern hemisphere.  
21 Such differences might be caused by experimental issues such as overestimated extraction  
22 efficiency or can be due to real temporal variability as the sampling seasons differed. The  
23 extraction efficiency has been estimated as 92.12 (±0.013)% (see Appendix) and was  
24 incorporated into the calculation of the original seawater concentration. With respect to the  
25 assumption of biological production as main production pathway it is more likely that due to  
26 the different sampling seasons less H<sub>2</sub> was produced in April than in October / November  
27 because of less microbial activity especially on the northern hemisphere in boreal winter.

28

### 29 **3.3.2 Isotopic composition of H<sub>2</sub>**

30 Additional information about H<sub>2</sub> sources comes from the analysis of the H<sub>2</sub> isotopic  
31 composition. In the literature only one experimental value of dissolved marine  $\delta\text{D}$  exists,  $\delta\text{D}$   
32 = -628 ‰ (Price et al. 2007, Rice et al. 2010), but the origin of this value is unclear and it is

1 based on unpublished data. Nevertheless, this value has been used as representative for  
2 oceanic emission in several global budget calculations (e.g. Price et al. 2007, Pieterse et al.  
3 2011). Other authors (e.g. Rahn et al. 2003, Rhee et al. 2006) used a theoretical value of  $-700$   
4 ‰, as expected for thermodynamic isotope equilibrium between  $H_2$  and  $H_2O$  based on the  
5 calculations of Bottinga (1969). The results presented here are the first well-documented  
6 experimental results for isotope analysis of dissolved  $H_2$  in seawater.

7 From the measurement of the isotopic composition of  $H_2$  in the headspace we calculate the  
8 isotopic composition of  $H_2$  that was originally dissolved in the sea water as described in  
9 section 2.4.3 and in the Appendix, using two different assumptions for fractionation between  
10 dissolved  $H_2$  and  $H_2$  in the gas phase. The results shown in Table 4 reveal  $\delta D$  values for the  
11 dissolved  $H_2$  that vary within a wide range of  $-112$  ‰ to  $-719$  ‰ for both fractionation  
12 scenarios. Interestingly,  $\delta D$  shows two distinct groups of samples that can be separated by the  
13 water temperature (Fig. 7b). In water masses with a temperature above  $21$  °C the  $\delta D$  values  
14 are  $(-629 \pm 54)$  ‰ ( $n = 14$ ), in water masses with a temperature of  $20$  °C or below  $\delta D$  values  
15 are  $(-249 \pm 88)$  ‰ ( $n = 8$ ). There is no correlation of  $\delta D$  with salinity (Fig. 7c), but the high  
16 temperature (and low  $\delta D$ ) waters show also a generally higher saturation than the low  
17 temperature (high  $\delta D$ ) waters (Fig. 7d).

18 The very depleted isotope signature of the  $H_2$  in the warmer water masses is consistent with  
19 the values expected for biological production. The slight enrichment compared to the value of  
20  $\approx -700$  ‰ that is expected for biologically produced  $H_2$  in equilibrium with ocean water  
21 (Bottinga, 1969, Walter et al., 2012) may be caused by a partial consumption within the  
22 water, which would enrich the remaining fraction. The relatively smooth distribution of the  
23 isotopic composition of  $H_2$  in the atmosphere strongly indicates that the contribution from  
24 atmospheric variability cannot be a main contributor of the isotope variations observed in  
25 dissolved  $H_2$ , even within the group of the depleted samples.

26 To our knowledge this is the first time that oceanic production of  $H_2$  has been directly  
27 attributed to biological processes by using isotope techniques. For the samples collected from  
28 warm surface waters, our results verify the general assumption of a biological production  
29 process as a main source of oceanic  $H_2$  to the atmosphere rather than photochemical or other  
30 sources (Herr et al. 1981, Conrad, 1988; Punshon and Moore, 2008, Moore et al. 2009). The  
31 dominance of biological formation at higher temperatures is qualitatively consistent with the  
32 general understanding of the temperature dependence of  $N_2$  fixation rates for  $N_2$  fixers such as

1 e.g. *Trichodesmium spec.*, which exhibit highest N<sub>2</sub> fixation rates within a temperature range  
2 between 24 °C to 30 °C (Breitbarth et al. 2007, Stal 2009). In fact, the saturations also show a  
3 correlation with temperature, but less clear than for δD (Fig. 7d), presumably due to  
4 simultaneous uptake and consumption processes in a complex microbial community.  
5 However, this clear attribution is only valid in water masses with higher temperatures and the  
6 unexpectedly high δD values in cooler waters indicate the influence of other processes. The  
7 isotopic enrichment that is expected for removal of H<sub>2</sub> (Chen et al., 2015, Rahn et al., 2003,  
8 Constant et al., manuscript in preparation) is highly unlikely to cause a shift of almost 400 ‰  
9 in δD from an assumed pure biological source, because in this case the removed fraction  
10 would have to be unrealistically large, as also recently argued for soil emitted H<sub>2</sub> (Chen et al.,  
11 2015). We suggest that a source of H<sub>2</sub> must exist in these surface waters, which produces H<sub>2</sub>  
12 that is out of isotope equilibrium with the water. This can be either one single source with an  
13 isotopic signature of approximately -250 ‰, or an even more isotopically enriched source that  
14 mixes with the depleted biological source.  
15 Punshon and Moore (2008a, and references therein), reported abiotic photochemical H<sub>2</sub>  
16 production from CDOM and small organic compounds such as acetaldehyde or syringic acid.  
17 Walter et al. (2013) indicated, that biologically active regions such as the Banc d'Arguin at  
18 the coast of Mauritania could act as a pool of precursors such as VOCs for atmospheric H<sub>2</sub>  
19 with high δD values. It is thus possible that abiotic photochemical production in the surface  
20 water might be an alternative source of H<sub>2</sub> excess, which is not isotopically equilibrated with  
21 water, especially in regions with high radiation and biological activity, and less N<sub>2</sub> fixation.  
22 Given the fact that the two groups of warm and cold waters are relatively well separated and  
23 there is not a continuous mixing curve between two end members, the explanation of a single  
24 different source seems more straightforward. Isotope analyses are a powerful tool to  
25 distinguish this source from biological production. Additional measurements are needed to  
26 determine the isotopic signature of such a source and investigate to which extend  
27 photochemical production contributes to the oceanic H<sub>2</sub> budget in colder water masses, and  
28 also update the current models. However, with an isotopic signature of approximately -250  
29 ‰, or an even more isotopically enriched, such a source would not significantly impact the  
30 current models.  
31 Based on their H<sub>2</sub> measurements, Moore et al. (2014) suggested a substantial underestimation  
32 of oceanic N<sub>2</sub> fixation, especially due to high H<sub>2</sub> supersaturations measured in the southern

1 hemisphere. By using direct measurements of N<sub>2</sub> fixation rates a systematic underestimation  
2 by approximately 60 % was also proposed by Großkopf et al. (2012) who suggested a global  
3 marine N<sub>2</sub> fixation rate of (177 ±8) Tg N a<sup>-1</sup>. In order to identify a possible significant  
4 mismatch between N<sub>2</sub> fixation rates and total marine H<sub>2</sub> production, we calculated the  
5 climatological global oceanic emissions from the GEMS database using the protocol of  
6 Pieterse et al. (2013), and an assumed mean oceanic H<sub>2</sub> source of 5 Tg a<sup>-1</sup> as given from  
7 global budget calculations. The estimated emission rates and distributions in the Atlantic  
8 Ocean (Fig. 8) are in line with the calculations of Moore et al. (2014), who reported H<sub>2</sub> sea-to-  
9 air fluxes mostly in the range of (10±5) mmol m<sup>-2</sup> a<sup>-1</sup> and an almost equal distribution  
10 between the hemispheres.

11 Westberry and Siegel (2006) estimated the global nitrogen fixation rate by *Trichodesmium*  
12 blooms by using satellite ocean color data at 42 Tg N a<sup>-1</sup> and an additional 20 Tg N a<sup>-1</sup> under  
13 non-bloom conditions, suggesting that *Trichodesmium* is likely the dominant organism in the  
14 global ocean new nitrogen budget. The good agreement between our measurements of H<sub>2</sub>  
15 concentrations and δD and the model results from the TM5 model indicate that the oceanic  
16 emissions of H<sub>2</sub> to the atmosphere are actually well represented in current atmospheric  
17 models (Pieterse et al. 2013 and references herein). The proposed underestimate of oceanic N<sub>2</sub>  
18 fixation and a possible additional H<sub>2</sub> release during this process seems already be  
19 incorporated in the current atmospheric budgets of H<sub>2</sub>. Thus, supposing that both an assumed  
20 total oceanic H<sub>2</sub> source of 5 Tg a<sup>-1</sup> to the atmosphere and a total global nitrogen fixation rate  
21 of approximately 177 Tg N a<sup>-1</sup> are correct, our calculations clearly support the suggestion of  
22 Großkopf et al. (2012) that N<sub>2</sub> fixers other than *Trichodesmium* have been severely  
23 underestimated in the global picture and that the oceanic release ratio of H<sub>2</sub> to fixed N<sub>2</sub> clearly  
24 needs more attention. Besides *Trichodesmium*, several other N<sub>2</sub>-fixing organisms are known  
25 for their potential to produce hydrogen (Wilson et al., 2010a; Falcón et al., 2002, 2004; Zehr  
26 et al., 2001; Kars et al., 2009; Barz et al., 2010), and even non-N<sub>2</sub>-fixing organisms might  
27 play a role (Lilley et al. 1982).

28

## 29 **4 Conclusions**

30 Identifying sources is important to consider budgets and gain insight in production and  
31 consumption processes. Although H<sub>2</sub> has been assumed reasonably to be produced mainly  
32 biologically in the oceans, direct evidence was lacking. Our results verify a biological

1 production as a main source of H<sub>2</sub> in oceanic surface water, especially in warmer water  
2 masses. As seen from the transects, local sources are difficult to spot due to their patchiness,  
3 this should be taken into account when planning the sampling strategy.  
4 The unexpectedly high  $\delta D$  values in colder temperate water masses indicate the significant  
5 influence of processes other than biological production, and additional information e.g. by  
6 isotopic composition is needed to distinguish and verify possible sources and supersaturations  
7 of dissolved oceanic H<sub>2</sub>. Especially the investigation of the isotopic composition of possible  
8 production pathways such as abiotic photochemical H<sub>2</sub> production needs further attention and  
9 should be an upcoming issue.

10 The pattern of mole fractions and isotopic composition of H<sub>2</sub> along a north–south Atlantic  
11 transect clearly depends on season and hemisphere and are consistent with previous published  
12 data and models. A possible significant underestimation of N<sub>2</sub> fixation as assumed by several  
13 authors could – providing a net H<sub>2</sub> release rate – go along with higher H<sub>2</sub> emissions. However,  
14 a comparison with the TM5 model and the calculation of the climatological global oceanic  
15 emissions based on GEMS database reveal that the oceanic contribution to the global H<sub>2</sub>  
16 budget is reasonable and in general reproduced well and therefore a proposed underestimation  
17 in the oceanic N<sub>2</sub> fixation seems already be corrected (from atmospheric considerations) in  
18 the current atmospheric budgets of H<sub>2</sub>. This also indicates, with respect to the proposed source  
19 different than biological production in colder temperate water masses, that such a source  
20 would probably not significantly impact the current models.

21 Besides the isotopic composition of photochemically produced H<sub>2</sub> the composition of N<sub>2</sub> fixer  
22 communities and the release ratio of H<sub>2</sub> to N<sub>2</sub> fixed needs more investigation to understand  
23 the general processes and distributions of oceanic H<sub>2</sub> in more detail.

24

## 25 **Acknowledgements**

26 We are very thankful to the crew of the RV *Polarstern* and RV *L'Atalante* for their friendly  
27 and professional help and support. This study was financed by the NWO (Netherlands  
28 Organization for Scientific Research), NWO project number 816.01.001, the EU FP7 project  
29 InGOS (GA number 284274), and the BMBF (Bundesministerium für Bildung und  
30 Forschung) project SOPRAN, grant FKZ 03F0462, grant 03F0611 and grant 03F0662.

31

## 1 **References**

- 2 Barz, M., Beimgraben, C., Staller, T., Germer, F., Opitz, F., Marquardt, C., Schwarz, C.,  
3 Gutekunst, K., Vanselow, K.H., Schmitz, R., LaRoche, J., Schulz, R., and Appel, J.:  
4 Distribution analysis of hydrogenases in surface waters of marine and freshwater  
5 environments, *PloS ONE*, 5(11), e13846, doi:10.1371/journal.pone.0013846, 2010.
- 6 Batenburg, A. M., Walter, S., Pieterse, G., Levin, I., Schmidt, M., Jordan, A., Hammer, S.,  
7 Yver, C., and Röckmann, T.: Temporal and spatial variability of the stable isotopic  
8 composition of atmospheric molecular hydrogen: observations at six EUROHYDROS  
9 stations, *Atmos. Chem. Phys.*, 11, 6985–6999, doi:10.5194/acp-11-6985-2011, 2011.
- 10 Battino, R.: The Ostwald coefficient of gas solubility, *Fluid Phase Equilib.*, 15, 231-240,  
11 [http://dx.doi.org/10.1016/0378-3812\(84\)87009-0](http://dx.doi.org/10.1016/0378-3812(84)87009-0), 1984
- 12 Bothe, H., Neuer, G., Kalbe, I., and Eisbrenner, G.: Electron donors and hydrogenase in  
13 nitrogen-fixing microorganisms, in: Stewart WDP, Gallon JR (eds) *Nitrogen fixation*.  
14 Academic Press, London, p 83–112, 1980.
- 15 Bothe, H., Schmitz, O., Yates, M. G., and Newton, W. E.: Nitrogen fixation and hydrogen  
16 metabolism in cyanobacteria, *MMBR*, 74(4), 529–51, doi:10.1128/MMBR.00033-10, 2010.
- 17 Breitbarth, E., Oshlies, A., and LaRoche, J.: Physiological constraints on the global  
18 distribution of *Trichodesmium* – effect of temperature on diazotrophy, *Biogeosciences*, 4, 53–  
19 61, 2007.
- 20 Bottinga, Y.: Calculated fractionation factors for carbon and hydrogen isotope exchange in  
21 the system calcite–carbon dioxide–graphite–methane–hydrogen–water vapour, *Geochim.*  
22 *Cosmochim. Ac.*, 33, 49–64, 1969.
- 23 Chen, Q., Popa, E.M., Batenburg, A.M., and Röckmann, T.: Isotopic signatures of production  
24 and uptake of H<sub>2</sub> by soil, *Atmos. Chem. Phys.*, 15, 13003–13021, doi:10.5194/acp-15-13003-  
25 2015, 2015
- 26 Conrad, R., and Seiler, W.: Methane and hydrogen in seawater (Atlantic Ocean), *Deep-Sea*  
27 *Res.*, 35(12), 1903–1917, 1988.
- 28 Constant, P., Walter, S., Batenburg, A.M., Liot, Q.; and Röckmann, T.: Kinetics and isotopic  
29 signature of the H<sub>2</sub> uptake activity of three Actinobacteria scavenging atmospheric H<sub>2</sub>, in  
30 preparation, 2015
- 31 Ehhalt, D.H., and Rohrer, F.: The tropospheric cycle of H<sub>2</sub>: a critical review, *Tellus B*, 61,  
32 500–535, 2009.

1 Erickson, D. J., and Taylor, J. A.: 3-D Tropospheric CO modeling: The possible influence of  
2 the ocean, *Geophys. Res. Lett.*, 19, 1955–1958, 1992

3 Falcón, L.I., Cipriano, F., Chistoserdov, A.Y., and Carpenter, E.J.: Diversity of diazotrophic  
4 unicellular cyanobacteria in the tropical North Atlantic Ocean, *Appl. Environ. Microbiol.*,  
5 68(11), 5760–5764, doi:10.1128/AEM.68.11.5760.2002, 2002.

6 Falcón, L.I., Carpenter, E.J., Cipriano, F., Bergman, B., and Capone, D.G.: N<sub>2</sub> fixation by  
7 unicellular bacterioplankton from the Atlantic and Pacific Oceans: Phylogeny and in situ  
8 rates, *Appl. Environ. Microbiol.*, 70(2), 765–770, doi:10.1128/AEM.70.2.765–770.2004,  
9 2004.

10 Feck, T., Groß, J.-U., and Riese, M.: Sensitivity of Arctic ozone loss to stratospheric H<sub>2</sub>O,  
11 *Geophys. Res. Lett.*, 35, L01803, doi:10.1029/2007GL031334, 2008.

12 Feilberg, K.L., Johnson, M.S., Bacak, A., Röckmann, T., and Nielsen, C.J.: Relative  
13 tropospheric photolysis rates of HCHO and HCDO measured at the European photoreactor  
14 facility, *J. Phys. Chem. A*, 111(37), 9034–9046, 2007.

15 Gerst, S., and Quay, P.: Deuterium component of the global molecular hydrogen cycle, *J.*  
16 *Geophys. Res.*, 106, 5021–5031, 2001.

17 Green, E.J., and Carritt, D.E.: New tables for oxygen saturation of seawater, *J. Mar. Res.*, 25,  
18 140-147, 1967

19 Großkopf, T., Mohr, W., Baustian, T., Schunck, H., Gill, D., Kuypers, M.M.M., Lavik, G.,  
20 Schmitz, R.A., Wallace, D.W.R., LaRoche, J.: Doubling of marine dinitrogen-fixation rates  
21 based on direct measurements, *Nature*, 488, 361–364, doi:10.1038/nature11338, 2012.

22 Hanschmann, T., Deneke, H., Roebeling, R., and Macke, A.: Evaluation of the shortwave  
23 cloud radiative effect over the ocean by use of ship and satellite observations, *Atmos. Chem.*  
24 *Phys.*, 12, 12243–12253, doi:10.5194/acp-12-12243-2012, 2012.

25 Hauglustaine, D.A., and Ehhalt, D.H.: A three-dimensional model of molecular hydrogen in  
26 the troposphere, *J. Geophys. Res.*, 107(D17), 4330–4346, doi:10.1029/2001JD001156, 2002.

27 Herr, F.L.: Dissolved hydrogen in Eurasian Arctic waters, *Tellus*, 36B, 55–66, 1984.

28 Herr, F.L., Scranton, M.I., and Barger, W.R.: Dissolved hydrogen in the Norwegian Sea:  
29 Mesoscale surface variability and deep-water distribution, *Deep-Sea Res.*, 28A(9), 1001–  
30 1016, 1981.

31 Herr, F.L., Frank, E.C., Leone, G.M., and Kennicutt, M.C.: Diurnal variability of dissolved  
32 molecular hydrogen in the tropical South Atlantic Ocean, *Deep-Sea Res.*, 31(1), 13–20, 1984.

1 Houweling, S., Dentener, F., and Lelieveld, J.: The impact of non-methane hydrocarbon  
2 compounds on tropospheric photochemistry, *J. Geophys. Res.*, 103(D9), 10673–10696,  
3 doi:10.1029/97JD03582, 1998.

4 Jacobson, M.Z., Colella, W.G., and Golden, D.M.: Cleaning the air and improving health with  
5 hydrogen fuel-cell vehicles, *Science*, 308, 1901–1905, 2005.

6 Jacobson, M.Z.: Effects of wind-powered hydrogen fuel cell vehicles on stratospheric ozone  
7 and global climate, *Geophys. Res. Lett.*, 35, L19803, doi:10.1029/2008GL035102, 2008.

8 Jordan, A. and Steinberg, B.: Calibration of atmospheric hydrogen measurements, *Atmos.*  
9 *Meas. Tech.*, 4, 509–521, doi:10.5194/amt-4-509-2011, 2011.

10 Kars, G., Gündüz, U., Yücel, M., Rakhely, G., Kovacs, K.L., & Eroğlu, İ.: Evaluation of  
11 hydrogen production by *Rhodobacter sphaeroides* O.U.001 and its *hupSL* deficient mutant  
12 using acetate and malate as carbon sources. *Int. J. Hydrogen Energ.*, 34(5), 2184–2190.  
13 Doi:10.1016/j.ijhydene.2009.01.016, 2009.

14 Knox, M., Quay, P.D., and Wilbur, D.: Kinetic isotopic fractionation during air-water gas  
15 transfer of O<sub>2</sub>, N<sub>2</sub>, CH<sub>4</sub>, and H<sub>2</sub>, *J. Geophys. Res.*, 97(C12), 20335-20343, 1992.

16 Kock, A., Gebhardt S., and Bange, H.W.: Methane emissions from the upwelling area off  
17 Mauritania (NW Africa), *Biogeosciences*, 5, 1119–1125, doi:10.5194/bg-5-1119-2008, 2008.

18 Krol, M., Houweling, S., Bregman, B., van den Broek, M., Segers, A., van Velthoven, P.,  
19 Peters, W., Dentener, F., and Bergamaschi, P.: The two-way nested global chemistry-  
20 transport zoom model TM5: Algorithm and applications, *Atmos. Chem. Phys*, 5(2), 417–432,  
21 doi:10.5194/acp-5-417-2005, 2005.

22 Lilley, M.D., Baross, J.A., and Gordon, L.I.: Dissolved hydrogen and methane in Sannieh  
23 Inlet, British Columbia, *Deep-Sea Res.*, 29(12A), 1471–1484, 0198–0149/82/121471–13,  
24 Printed in Great Britain, Pergamon Press Ltd., 1982.

25 Longhurst, A.R.: *Ecological Geography of the Sea*, 398 pp., Academic, San Diego,  
26 California, 1998.

27 Moore, R.M., Punshon, S., Mahaffey, C., and Karl, D.: The relationship between dissolved  
28 hydrogen and nitrogen fixation in ocean waters, *Deep-Sea Res.*, 56, 1449–1458,  
29 doi:10.1016/j.dsr.2009.04.008, 2009.

30 Moore, R.M., Kienast, M., Fraser, M., Cullen, J.J., Deutsch, C., Dutkiewicz, S., Follows, M.  
31 J., and Somes, C.J.: Extensive hydrogen supersaturations in the western South Atlantic Ocean  
32 suggest substantial underestimation of nitrogen fixation, *J. Geophys. Res. Oceans*, 119, 4340–

1 4350, doi:10.1002/2014JC010017, 2014.

2 Nilsson, E., Johnson, M.S., Taketani, F., Matsumi, Y., Hurley, M.D., and Wallington, T.J.:  
3 Atmospheric deuterium fractionation: HCHO and HCDO yields in the CH<sub>2</sub>DO + O<sub>2</sub> reaction,  
4 *Atmos. Chem. Phys.*, 7, 5873–5881, 2007.

5 Nilsson, E.J.K., Andersen, V.F., Skov, H., and Johnson, M.S.: Pressure dependence of the  
6 deuterium isotope effect in the photolysis of formaldehyde by ultraviolet light, *Atmos. Chem.*  
7 *Phys.*, 10, 3455–3463, 2010.

8 Novelli, P.C., Lang, P.M., Masarie, K.A., Hurst, D.F., Myers, R., and Elkins, J.W.: Molecular  
9 hydrogen in the troposphere: Global distribution and budget, *J. Geophys. Res.*, 104, 30427–  
10 30444, 1999.

11 Pieterse, G., Krol, M.C., and Röckmann, T.: A consistent molecular hydrogen isotope  
12 chemistry scheme based on an independent bond approximation, *Atmos. Chem. Phys.*, 9,  
13 8503–8529, 2009.

14 Pieterse, G., Krol, M.C., Batenburg, A.M., Steele, L.P., Krummel, P.B., Langenfelds, R.L.,  
15 and Röckmann, T.: Global modelling of H<sub>2</sub> mixing ratios and isotopic compositions with the  
16 TM5 model, *Atmos. Chem. Phys.*, 11(14), 7001–7026, doi:10.5194/acp-11-7001-2011, 2011.

17 Pieterse, G., Krol, M.C., Batenburg, A.M., Brenninkmeijer, C.A.M., Popa, M.E., O’Doherty,  
18 S., Grant, A., Steele, L.P., Krummel, P.B., Langenfelds, R.L., Wang, H.J., Vermeulen, A.T.,  
19 Schmidt, M., Yver, C., Jordan, A., Engel, A., Fisher, R.E., Lowry, D., Nisbet, E.G., Reimann,  
20 S., Vollmer, M.K., Steinbacher, M., Hammer, S., Forster, G., Sturges, W.T., and Röckmann,  
21 T.: Reassessing the variability in atmospheric H<sub>2</sub> using the two-way nested TM5 model, *J.*  
22 *Geophys. Res. Atmos.*, 118, 3764–3780, doi:10.1002/jgrd.50204, 2013.

23 Popa, M.E., Vollmer, M.K., Jordan, A., Brand, W.A., Pathirana, S.L., Rothe, M., Röckmann,  
24 T.: Vehicle emissions of greenhouse gases and related tracers from a tunnel study: CO:CO<sub>2</sub>,  
25 N<sub>2</sub>N<sub>2</sub>O:CO<sub>2</sub>, CH<sub>4</sub>:CO<sub>2</sub>, O<sub>2</sub>:CO<sub>2</sub> ratios, and the stable isotopes <sup>13</sup>C and <sup>18</sup>O in CO<sub>2</sub> and CO,  
26 *Atmos. Chem. Phys.*, 14, 2105–2123, doi:10.5194/acp-14-2105-2014, 2014.

27 Popa, M.E., Segers, A.J., van der Gon, H.A.C.D., Krol, M.C., Visschedijk, A.J.H., Schaap,  
28 M., and Rockmann, T.: Impact of a future H<sub>2</sub> transportation on atmospheric pollution in  
29 Europe, *Atmos Environ*, 113, 208-222, doi:10.1016/j.atmosenv.2015.03.022, 2015.

30 Prather, M.J.: An environmental experiment with H<sub>2</sub>?, *Science*, 302, 581–582, 2003.

31 Price, H., Jaegle, L., Rice, A., Quay, P., Novelli, P.C., Gammon, R.: Global budget of  
32 molecular hydrogen and its deuterium content: constraints from ground station, cruise, and

1 aircraft observations, *J. Geophys. Res.*, 112, D22108, doi:10.1029/2006JD008152, 2007.

2 Punshon, S., Moore, R.M., and Xie, H.: Net loss rates and distribution of molecular hydrogen  
3 ( $H_2$ ) in mid-latitude coastal waters, *Mar. Chem.*, 105(1–2), 129–139,  
4 doi:10.1016/j.marchem.2007.01.009, 2007.

5 Punshon, S., and Moore, R.: Photochemical production of molecular hydrogen in lake water  
6 and coastal seawater, *Mar. Chem.*, 108(3–4), 215–220, doi:10.1016/j.marchem.2007.11.010,  
7 2008a.

8 Punshon, S., and Moore, R.M.: Aerobic hydrogen production and dinitrogen fixation in the  
9 marine cyanobacterium *Trichodesmium erythraeum* IMS101, *Limnol. Oceanogr.*, 53(6),  
10 2749–2753, 2008b.

11 Rahn, T., Kitchen, N., and Eiler, J.M.: D/H ratios of atmospheric  $H_2$  in urban air: Results  
12 using new methods for analysis of nano-molar  $H_2$  samples, *Geochim. Cosmochim. Acta*, 66,  
13 2475–2481, 2002.

14 Rahn, T., Eiler, J.M., Boering, K.A., Wennberg, P.O., McCarthy, M.C., Tyler, S., Schauffler,  
15 S., Donnelly, S., and Atlas, E.: Extreme deuterium enrichment in stratospheric hydrogen and  
16 the global atmospheric budget of  $H_2$ , *Nature*, 424, 918–921, 2003.

17 Rhee, T.S., Mak, J., Röckmann, T., and Brenninkmeijer, C.A.M.: Continuous-flow isotope  
18 analysis of the deuterium/hydrogen ratio in atmospheric hydrogen, *Rapid Commun. Mass*  
19 *Spectrom.*, 18 (3), 299–306, doi: 10.1002/rcm.1309, 2004.

20 Rhee, T.S., Brenninkmeijer, C.A.M., and Röckmann, T.: The overwhelming role of soils in  
21 the global atmospheric hydrogen cycle, *Atmos. Chem. Phys.*, 6, 1611–1625, 2006.

22 Rice, A., Quay, P., Stutsman, J., Gammon, R., Price, H., and Jaegle, L.: Meridional  
23 distribution of molecular hydrogen and its deuterium content in the atmosphere, *J. Geophys.*  
24 *Res.*, 115, D12306, doi:10.1029/2009JD012529, 2010.

25 Robinson, C., Holligan, P., Jickels, T., and Lavender, S.: The Atlantic Meridional Transect  
26 Programme (1995 – 2012), *Deep-Sea Res. II*, 56, 895–898, doi:10.1016/j.dsr2.2008.10.005,  
27 2009.

28 Röckmann, T., Rhee, T.S., and Engel, A.: Heavy hydrogen in the stratosphere, *Atmos. Chem.*  
29 *Phys.*, 3, 2015–2023, 2003.

30 Röckmann, T., Gómez Álvarez, C.X., Walter, S., van Veen, C., Wollny, A.G., Gunthe, S.S.,  
31 Helas, G., Pöschl, U., Keppler, F., Greule, M., and Brand, W.A.: The isotopic composition of

1 H<sub>2</sub> from wood burning – dependency on combustion efficiency, moisture content and  $\delta D$  of  
2 local precipitation, *J. Geophys. Res.*, 115, D17308, doi:10.1029/2009JD013188, 2010a.

3 Röckmann, T., Walter, S., Bohn, B., Wegener, R., Spahn, H., Brauers, T., Tillmann, R.,  
4 Schlosser, E., Koppmann, R., and Rohrer, F.: Isotope effect in the formation of H<sub>2</sub> from  
5 H<sub>2</sub>CO studied at the atmospheric simulation chamber SAPHIR, *Atmos. Chem. Phys.*, 10,  
6 5343–5357, 2010b.

7 Schlitzer, R., *Ocean Data View* 4, <http://odv.awi.de>, 2012.

8 Schultz, M.G., Diehl, T., Brasseur, G.P., and Zittel, W.: Air pollution and climate–forcing  
9 impacts of a global hydrogen economy, *Science*, 302, 624–627, 2003.

10 Schütz, K., Happe, T., Troshina, O., Lindblad, P., Leitão, E., Oliveira, P., and Tamagnini, P.:  
11 Cyanobacterial H<sub>2</sub> production – a comparative analysis, *Planta*, 218(3), 350–359,  
12 doi:10.1007/s00425–003–1113–5, 2004.

13 Scranton, M., Jones, M., and Herr, F.L.: Distribution and variability of hydrogen in the  
14 Mediterranean Sea, *J. Mar. Res.* 40: 873–891, 1982.

15 Scranton, M.I.: The role of the cyanobacterium *Oscillatoria (Trichodesmium) thiebautii* in the  
16 marine hydrogen cycle, *Mar. Ecol.*, 11(1), 79–87, 1983.

17 Seiler, W., and Schmidt, U.: Dissolved non–conservative gases in seawater. In: Goldberg ED  
18 (ed) *The sea*, Vol 5. John Wiley & Sons, New York, p 219–243, 1974.

19 Stal, L.J.: Is the distribution of nitrogen–fixing cyanobacteria in the oceans related to  
20 temperature?, *Environmental Microbiology*, 11(7), 1632–1645, doi:10.1111/j.1758–  
21 2229.2009.00016.x, 2009.

22 Tamagnini, P., Leitão, E., Oliveira, P., Ferreira, D., Pinto, F., Harris, D. J., Heidorn, T., and  
23 Lindblad, P.: Cyanobacterial hydrogenases: diversity, regulation and applications, *FEMS*  
24 *microbiology reviews*, 31(6), 692–720, doi:10.1111/j.1574–6976.2007.00085.x, 2007.

25 Tromp, T.K., Shia, R.-L., Allen, M., Eiler, J.M., and Yung, Y.L.: Potential environmental  
26 impact of a hydrogen economy on the stratosphere, *Science*, 300, 1740–1742, 2003.

27 Vollmer, M.K., Walter, S., Bond, S.W., Soltic, P., and Röckmann, T.: Molecular hydrogen  
28 (H<sub>2</sub>) emissions and their isotopic signatures (H/D) from a motor vehicle: implications on  
29 atmospheric H<sub>2</sub>, *Atmos. Chem. Phys.*, 10, 5707–5718, doi:10.5194/acp–10–5707–2010, 2010.

30 Walter, S., Laukenmann, S., Stams, A.J.M., Vollmer, M.K., Gleixner, G., and Röckmann, T.:  
31 The stable isotopic signature of biologically produced molecular hydrogen (H<sub>2</sub>),  
32 *Biogeosciences* 9, 4115–4123, doi:10.5194/bg–9–4115–2012, 2012.

1 Walter, S., Kock, A., and Röckmann, T.: High-resolution measurements of atmospheric  
2 molecular hydrogen and its isotopic composition at the West African coast of Mauritania,  
3 Biogeosciences, 10, 3391–3403, doi:10.5194/bg-10-3391-2013, 2013.

4 Warwick, N.J., Bekki, S., Nisbet, E.G., and Pyle, J.A.: Impact of a hydrogen economy on the  
5 stratosphere and troposphere studied in a 2-D model, Geophys. Res. Lett., 31, L05107,  
6 doi:10.1029/2003GL019224, 2004.

7 Westberry, T.K., and Siegel, D.A.: Spatial and temporal distribution of *Trichodesmium*  
8 blooms in the world's oceans, Global Biogeochem. Cycles, 20, GB4016,  
9 doi:10.1029/2005GB002673, 2006.

10 Wiesenburg, D.A., and Guinasso, N.L.: Equilibrium solubilities of methane, carbon  
11 monoxide, and hydrogen in water and sea water, J. Chem. Eng. Data, 1979, 24 (4), pp 356–  
12 360, doi:10.1021/je60083a006, 1979.

13 Wilson, S.T., Foster, R.A., Zehr, J.P., and Karl, D.M.: Hydrogen production by  
14 *Trichodesmium erythraeum*, *Cyanothece* sp., and *Crocospaera watsonii*, Aquat. Microb.  
15 Ecol., 59(2), 197–206, doi:10.3354/ame01407, 2010a.

16 Wilson, S.T., Tozzi, S., Foster, R.A., Ilikchyan, I., Kolber, Z.S., Zehr, J.P., and Karl, D.M.:  
17 Hydrogen cycling by the unicellular marine diazotrophs *Crocospaera watsonii* strain  
18 WH8501, Appl. Environ. Microb., 76(20), 6797–803, doi:10.1128/AEM.01202-10, 2010b.

19 Wilson, S.T., del Valle, D.A., Robidart, J.C., Zehr, J.P., and Karl, D.M.: Dissolved hydrogen  
20 and nitrogen fixation in the oligotrophic North Pacific Subtropical Gyre, Environ. Microbiol.  
21 Rep., 5(5), 697–704, doi: 10.1111/1758-2229.12069, 2013.

22 Yashiro, H., Sudo, K., Yonemura, S., and Takigawa, M.: The impact of soil uptake on the  
23 global distribution of molecular hydrogen: chemical transport model simulation, Atmos.  
24 Chem. Phys., 11, 6701–6719, doi:10.5194/acp-11-6701-2011, 2011.

25 Yonemura, S., Kawashima, S., and Tsuruta, H.: Carbon monoxide, hydrogen, and methane  
26 uptake by soils in a temperate arable field and a forest, J. Geophys. Res. 105, 14347–14362,  
27 DOI: 10.1029/1999JD901156, 2000.

28 Yver, C.E., Pison, I.C., Fortems-Cheiney, A., Schmidt, M., Chevallier, F., Ramonet, M.,  
29 Jordan, A., Søvde, O.A., Engel, A., Fisher, R.E., Lowry, D., Nisbet, E.G., Levin, I., Hammer,  
30 S., Necki, J., Bartyzel, J., Reimann, S., Vollmer, M.K., Steinbacher, M., Aalto, T., Maione,  
31 M., Arduini, J., O'Doherty, S., Grant, A., Sturges, W.T., Forster, G.L., Lunder, C.R.,  
32 Privalov, V., Paramonova, N., Werner, A., and Bousquet, P.: A new estimation of the recent

1 tropospheric molecular hydrogen budget using atmospheric observations and variational  
2 inversion, *Atmos. Chem. Phys.*, 11, 3375–3392, doi:10.5194/acp-11-3375-2011, 2011.

3 Zehr, J.P., Waterbury, J.B., Turner, P.J., Montoya, J.P., Omoregie, E., Steward, G.F., Hansen,  
4 A., Karl, D.M.: Unicellular cyanobacteria fix N<sub>2</sub> in the subtropical North Pacific Ocean.

5 *Nature*, 412(6847), 635–638, 2001.

6

7

1  
2  
3  
4

Table 1: Overview of sample distribution during the cruises: type A are discrete atmospheric samples, type H are headspace samples extracted from the surface water. The sample numbers in brackets give the number of measured samples in the northern (NH) and southern (SH) hemisphere.

Cruise	Date	Position (start – end)	Nr. of Samples (NH / SH)	Type
ANT-XXIV/4	18.04. – 20.05.2008	59.15 °W / 46.13 ° S – 06.21 °W / 47.96 °N	95 (44 NH / 51 SH)	A
ANT-XXV/5	11.04. – 24.05.2009	50.99 °W / 40.82 ° S – 23.05 °W / 16.55 °N	91 (30 NH / 61 SH)	A
ANT XXVI/1	16.10. – 25.11.2009	12.05 °W / 37.96 °N – 47.28 °W / 37.43 ° S	60 (29 NH / 31 SH)	A
ANT XXVI/4	07.04. – 17.05.2010	58.14 °W / 43.75 ° S – 04.46 °E / 53.15 °N	114 (56 NH / 58 SH)	A
ANT XXVI/4	07.04. – 17.05.2010	32.53 °W / 18.79 ° S – 13.00 °W / 36.54 °N	16 (10 NH / 6 SH)	H
L'Atalante ATA-3	03.02. – 20.02.2008	17.83 °N / 16.56 °W – 17.60 °N / 24.24 °W	6 (6N H / 0 SH)	H

5  
6  
7  
8

1

Table 2: Hemispheric means of atmospheric H<sub>2</sub> and its isotopic composition along the four meridional Atlantic transects

Cruise		Southern Hemisphere				Northern Hemisphere			
		IRMS – H <sub>2</sub> mole fraction [ppb]	δD [‰]	RGA – H <sub>2</sub> mole fraction [ppb]	RGA – CO mole fraction [ppb]	IRMS – H <sub>2</sub> mole fraction [ppb]	δD [‰]	RGA – H <sub>2</sub> mole fraction [ppb]	RGA – CO mole fraction [ppb]
ANT- XXI/4 April 2008	mean	543.4±7.3	145.4±5.3	No data	No data	544.1±9.8	118.6±3.9	No data	No data
	range	528.8 – 568.5	135.4 – 155.7			522.0 – 567.8	110.4 – 130.9		
	<i>n</i>	49 (2 values excluded)	49 (2 values excluded)			44	44		
ANT- XXV/5 April 2009	mean	533.9±38.7	140.5±21.1	520.4±24.0	59.9±17.7	532.94±19.73	121.28±7.09	526.18±12.6	112.67±21.3
	range	350.2 – 631.9	20.9 – 166.1	432.5 – 545.1	43.6 – 119.6	466.9 – 560.3	89.1 – 130.9	508.9 – 564.1	76.9 – 190.5
	<i>n</i>	60 (2 values excluded)	60 (2 values excluded)	21	21	28 (2 values excluded)	28 (2 values excluded)	29	29
ANT XXVI/1 October 2009	mean	548.5±6.8	143.2±4.2	546.4±7.4	59.9±10.5	532.04±10.65	133.94±4.43	526.02±10.53	76.73±7.43
	range	535.9 – 563.4	135.5 – 149.3	531.4 – 563.0	47.7 – 85.8	501.1 – 551.7	123.5 – 141.7	494.2 – 548.8	65.4 – 96.1
	<i>n</i>	30 (1 value excluded)	30 (1 value excluded)	49	49	29	29	46	46
ANT XXVI/4 April 2010	mean	541.6±16.3	143.7±11.5	525.1±29.1	47.2±8.8	539.4±14.8	116.2±11.5	507.8±15.7	120.8±11.2
	range	496.0 – 579.6	89.3 – 161.8	481.5 – 696.8	36.2 – 121.8	505.5 – 564.6	93.8 – 146.6	481.3 – 603.8	72.7 – 146.1
	<i>n</i>	58	58	617	617	56	56	1339	1339

2

3

4

5

6

7

8

9

1 Table 3: Overview of means of atmospheric H<sub>2</sub> and its isotopic composition along the five high-resolution transects of ANT-XXV/5,  
 2 including the standard deviation and the range

Transect (latitude)		Mole fraction [ppb]	δD [‰]
40.8° S / 38.9° S <i>n</i> = 12	mean	515.5±37.7	141.4±6.2
	range	448.4 – 566.9	129.3 – 151.0
33.0° S / 30.8° S <i>n</i> = 12	mean	521.4±53.3	152.9±5.9
	range	350.2 – 551.9	142.8 – 166.1
23.5° S / 15.7° S <i>n</i> = 32	mean	536.9±38.4	144.1±41.4
	range	392.9 – 631.9	20.91 – 322.45
2.0° S / 3.2° N <i>n</i> = 11	mean	537.5±36.2	119.5±12.6
	range	466.9 – 592.2	89.1 – 135.5
9.9° N / 16.2° N <i>n</i> = 21	mean	537.0±12.2	122.5±3.0
	range	511.0 – 560.3	118.4 – 131.0

3

4

1 Table 4: overview of headspace sample results from the ANT-XXVI/4 cruise (2010) and the L'Atalante ATA-3 (2008).:  $\chi_h$  is the measured  
2 mole fraction of the headspace in parts per billion (ppb = nmole mole<sup>-1</sup>),  $\chi_a$  is the corresponding atmospheric mole fraction in ppb,  $\delta D_h$  and  
3  $\delta D_a$  is the measured isotopic composition in permill [‰]. The H<sub>2</sub> equilibrium concentration  $c_{sat}(H_2)$  was determined by using the equations  
4 from Wiesenburg and Guinasso (1979), the initial dissolved H<sub>2</sub> concentration  $c_{w0}$  is calculated as given in Appendix I, and the excess  $\Delta H_2$  is  
5 the difference between them.  $\delta_{w0\ SC1}$  and  $\delta_{w0\ SC2}$  show the two scenarios to derive the initial isotope delta of dissolved H<sub>2</sub>.  $S_{(H_2)}$  is the  
6 saturation of H<sub>2</sub> in the surface water. The calculated extraction efficiency was 92.12 (±0.013)%. The calculations are given in the Appendix  
7 in more detail.

Date / Time [UTC]	Sampling position	$\chi_a$ [ppb]	$\delta D_a$ [‰]	$\chi_h$ [ppb]	$\delta D_h$ [‰]	$c_{sat}(H_2)$ [nmol L <sup>-1</sup> ]	$c_{w0}$ [nmol L <sup>-1</sup> ]	$\Delta(H_2)$ [nmol L <sup>-1</sup> ]	$\delta_{w0\ SC1}$ [‰]	$\delta_{w0\ SC2}$ [‰]	$S_{(H_2)}$ [%]
21.04.2010 15:15	-18.79 °N -32.53 °E	562.0	148.5	653.3	-37.3	0.35	1.68	1.32	-536.2	-535.6	475
22.04.2010 15:24	-15.91 °N -30.49 °E	524.2	134.5	750.6	-138.6	0.33	2.89	2.57	-654.8	-654.4	880
23.04.2010 15:21	-13.06 °N -28.51 °E	551.6	144.3	754.4	-125.1	0.35	2.91	3.57	-602.9	-602.5	841
24.04.2010 15:36	-10.71 °N -26.92 °E	522.0	153.2	797.0	-151.2	0.33	3.52	3.19	-605.6	-605.2	1074
25.04.2010 15:24	-7.97°N -25.02°E	542.9	154.7	674.8	-59.4	0.34	1.97	1.63	-566.1	-565.6	581
26.04.2010 15:12	-5.16°N -23.11°E	517.8	149.7	584.5	9.2	0.32	0.83	0.51	-654.0	-653.6	256
28.04.2010 13:54	1.78 °N -23.00 °E	540.9	144.4	619.8	-33.1	0.34	1.27	0.93	-682.1	-681.8	376
29.04.2010 14:21	4.99 °N -23.00 °E	562.8	114.2	615.9	-11.7	0.35	1.25	0.89	-575.4	-574.9	353
30.04.2010 14:15	8.07 °N -23.00 °E	550.6	118.6	591.1	-0.6	0.35	0.94	0.60	-680.8	-680.5	271
02.05.2010 14:39	14.55 °N -23.68 °E	541.3	110.5	603.3	-15.0	0.35	1.13	0.78	-680.7	-680.4	324
04.05.2010 13:39	17.61 °N -24.75 °E	523.2	121.5	686.5	-83.6	0.34	2.27	1.93	-630.8	-630.3	674
05.05.2010 13:21	20.26 °N -22.86 °E	559.0	125.7	667.9	-55.3	0.36	2.05	1.69	-572.6	-572.2	566
06.05.2010 12:30	23.12 °N -20.66 °E	550.7	104.3	586.6	-1.1	0.36	0.93	0.57	-719.3	-719.0	258
07.05.2010 12:18	26.07 °N -17.50 °E	539.8	108.9	575.3	20.3	0.35	0.79	0.43	-645.2	-644.8	221
09.05.2010 12:51	33.60 °N -13.86 °E	546.8	104.6	624.2	21.0	0.37	1.51	1.14	-327.2	-326.4	410
10.05.2010 12:55	36.53 °N -13.01°E	531.8	107.8	571.6	62.0	0.36	0.77	0.41	-230.2	-229.3	213
09.02.2008 16:05	16.91°N -16.82°E	527.2	118.4	141.7	-224.09	0.35	1.57	1.22	-221.8	-221.0	446
11.02.2008 17:58	18.77 °N -16.81 °E	538.5	115.3	550.4	-383.39	0.36	5.91	5.54	-381.6	-380.9	1628
15.02.2008 10:27	17.93 °N -16.38 °E	536.8	112.2	138.8	-114.85	0.36	1.79	1.42	-112.2	-111.3	492
16.02.2008 6:05	17.72 °N -16.69 °E	548.4	120.0	20.3	-180.51	0.37	0.50	0.13	-179.0	-178.2	135
16.02.2008 17:41	18.01 °N -17.01 °E	548.4	120.0	31.0	-218.73	0.37	0.72	0.35	-217.3	-216.5	194
18.02.2008 18:22	18.00 °N -23.00 °E	541.8	126.5	48.9	-321.61	0.36	1.16	0.80	-320.4	-319.7	322

## 1 Figure captions

2 Figure 1: a) cruise tracks of the *RV Polarstern*, dots indicate positions of discrete atmospheric air sampling, b) positions of surface water  
3 headspace sampling during ANT-XXVI/4 ( $n = 16$ , green dots) and the *RV L'Atalante* ATA-3 cruise ( $n = 6$ , black dots)

4 Figure 2: Experimental setup for headspace sampling, a) sampling of the surface water into the glass vessel, connected to the Niskin bottle  
5 rosette, b) scheme of the experimental setup

6 Figure 3: Comparing the  $H_2$  mole fractions [ppb] measured with the isotopic experimental setup (x-axis) and the Peak Performer 1 RGA (y-  
7 axis) during ANT-XXVI/1 (red labeled) and ANT-XXV/5 (yellow labeled),  $y = 0.979x + 3.96$ ,  $R^2 = 0.81$ ,  $n = 147$

8 Figure 4:  $\delta D (H_2)$  [‰] (first column),  $H_2$  mole fraction [ppb] (second column), and CO mole fraction [ppb] (third column), along the  
9 meridional cruise tracks of *RV Polarstern*, the mole fraction and  $\delta D$  of  $H_2$  are measured by IRMS, the CO mole fraction by RGA

10 Figure 5: Comparison of measurement results of  $H_2$  and CO mole fractions and  $\delta D$  with TM5 model results (given in red). Data are shown  
11 against latitude. The blue markers show results of flask samples, the green markers represent the continuous in-situ measurements  
12 (performed with the peak performer instrument on-board). CO has not been analysed in the flasks sampled during the last cruise. The model  
13 data were interpolated at the place and time of sampling or measurements.

14 Figure 6: a)  $H_2$  mole fraction [ppb] (black) and  $\delta D$  [‰] (red) along the ANT-XXV/5 high-resolution transect  $24^\circ S$ – $15^\circ S$ ; b) Keeling plot of  
15 the samples along the high-resolution transect north of  $18^\circ S$ . The three trend lines indicate the range of the Keeling plot analysis that was  
16 applied to determine the source signature.

17  
18 Figure 7:

19 a)  $H_2$  saturation in the surface water (color coded) along the *RV Polarstern* cruise track of ANT-XXVI/4 and the *RV L'Atalante* cruise ATA-  
20 3, with maxima around the Cape Verde islands and  $10$ – $15^\circ S$ . Note: each sample is represented by a single dot.

21 b) Comparing the  $\delta D (H_2)$  at different water temperatures, the respective  $H_2$  saturation are color coded, sample dots marked with a diamond  
22 belong to the *RV L'Atalante* cruise, sample dots without to the ANT-XXVI/4 cruise;  $y = -35.2x + 360.9$ ,  $R^2 = 0.66$ ,  $n = 22$

23 c) Distribution of  $\delta D (H_2)$  (color coded) in correlation between water temperature and salinity

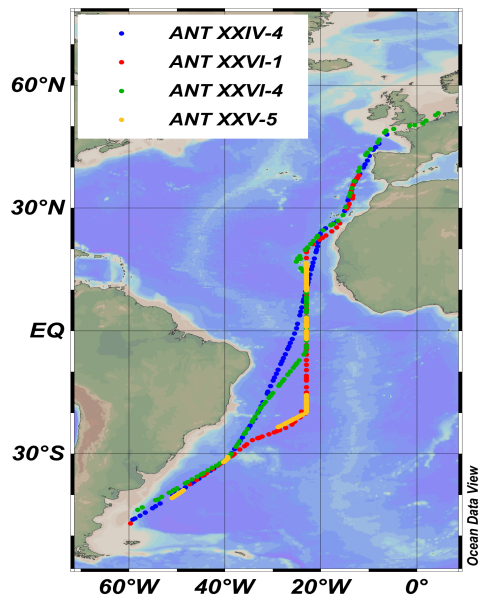
24 d) Correlation between water temperature and  $H_2$  saturation, the  $\delta D (H_2)$  is color-coded, the exceptional high saturation has been excluded  
25 from the correlation calculation,  $y = 0.26x - 2.79$ ,  $R^2 = 0.22$ ,  $n = 21$

26 Figure 8: Oceanic  $H_2$  emissions used in the TM5 model simulations ( $mmol m^{-2} a^{-1}$ , based on the distribution provided by the project GEMS  
27 (Global and regional Earth-system (Atmosphere) Monitoring using Satellite and in-situ data) and scaled to a total oceanic source of  $5 Tg a^{-1}$   
28 (Pieterse et al. (2013))

29  
30

1

a)



b)

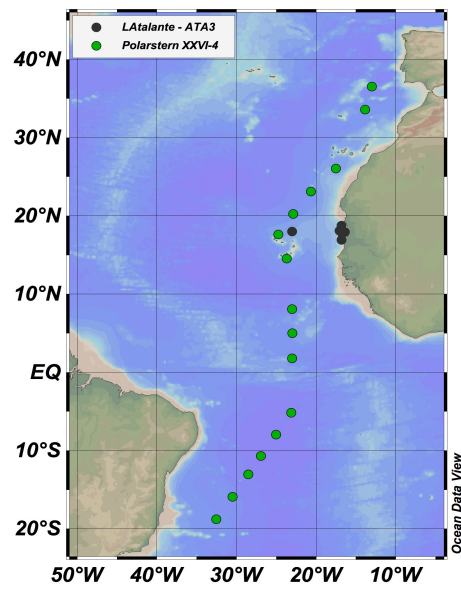


Figure 1: a) cruise tracks of the *RV Polarstern*, dots indicate positions of discrete atmospheric air sampling, b) positions of surface water headspace sampling during ANT-XXVI/4 ( $n = 16$ , green dots) and the *RV L'Atalante* ATA-3 cruise ( $n = 6$ , black dots)

2

3

4

1

a)



b)

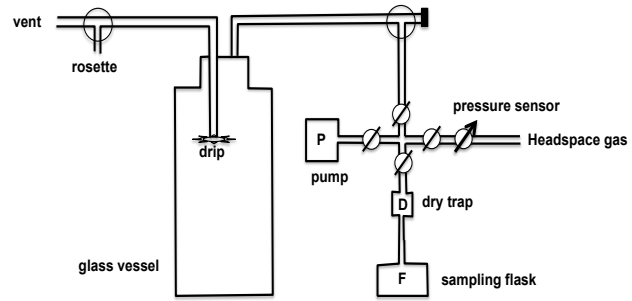


Figure 2: Experimental setup for headspace sampling, a) sampling of the surface water into the glass vessel, connected to the Niskin bottle rosette, b) scheme of the experimental setup

2

3

1

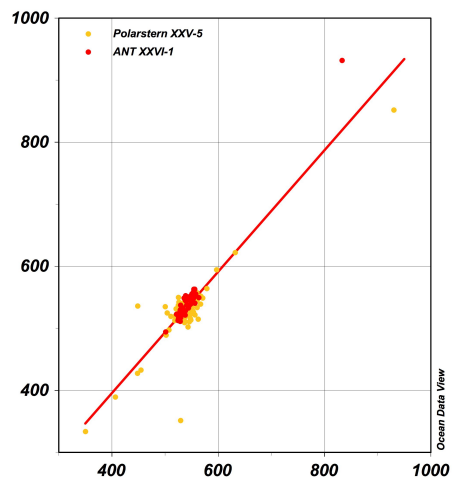


Figure 3: Comparing the H<sub>2</sub> mole fractions [ppb] measured with the isotopic experimental setup (x-axis) and the Peak Performer 1 RGA (y-axis) during ANT-XXVI/1 (red labeled) and ANT-XXV/5 (yellow labeled),  $y = 0.979x + 3.96$ ,  $R^2 = 0.81$ ,  $n = 147$

2

3

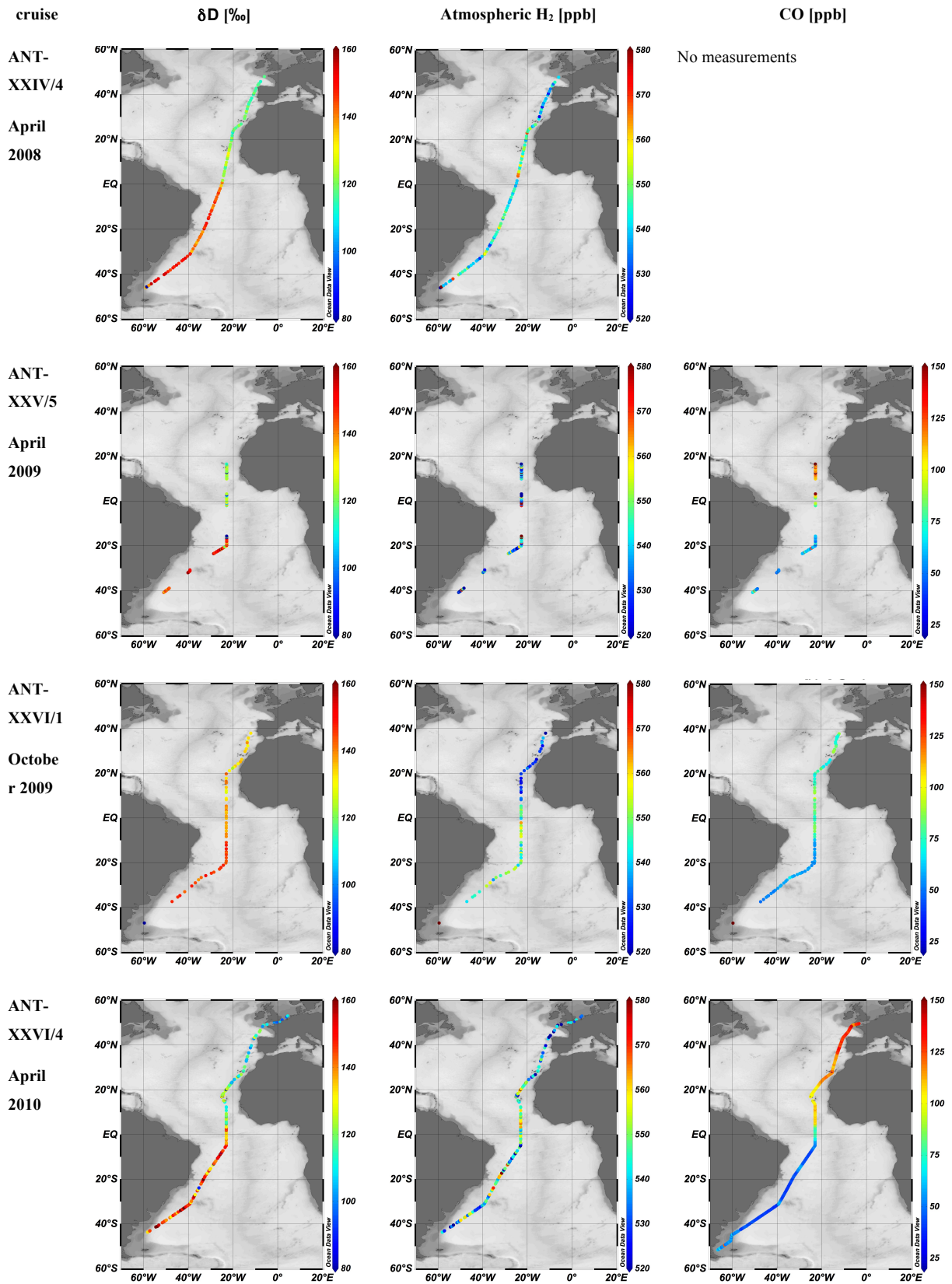


Figure 4:  $\delta D$  ( $H_2$ ) [‰] (first column),  $H_2$  mole fraction [ppb] (second column), and CO mole fraction [ppb] (third column), along the meridional cruise tracks of *RV Polarstern*, the mole fraction and  $\delta D$  of  $H_2$  are measured by IRMS, the CO mole fraction by RGA

1

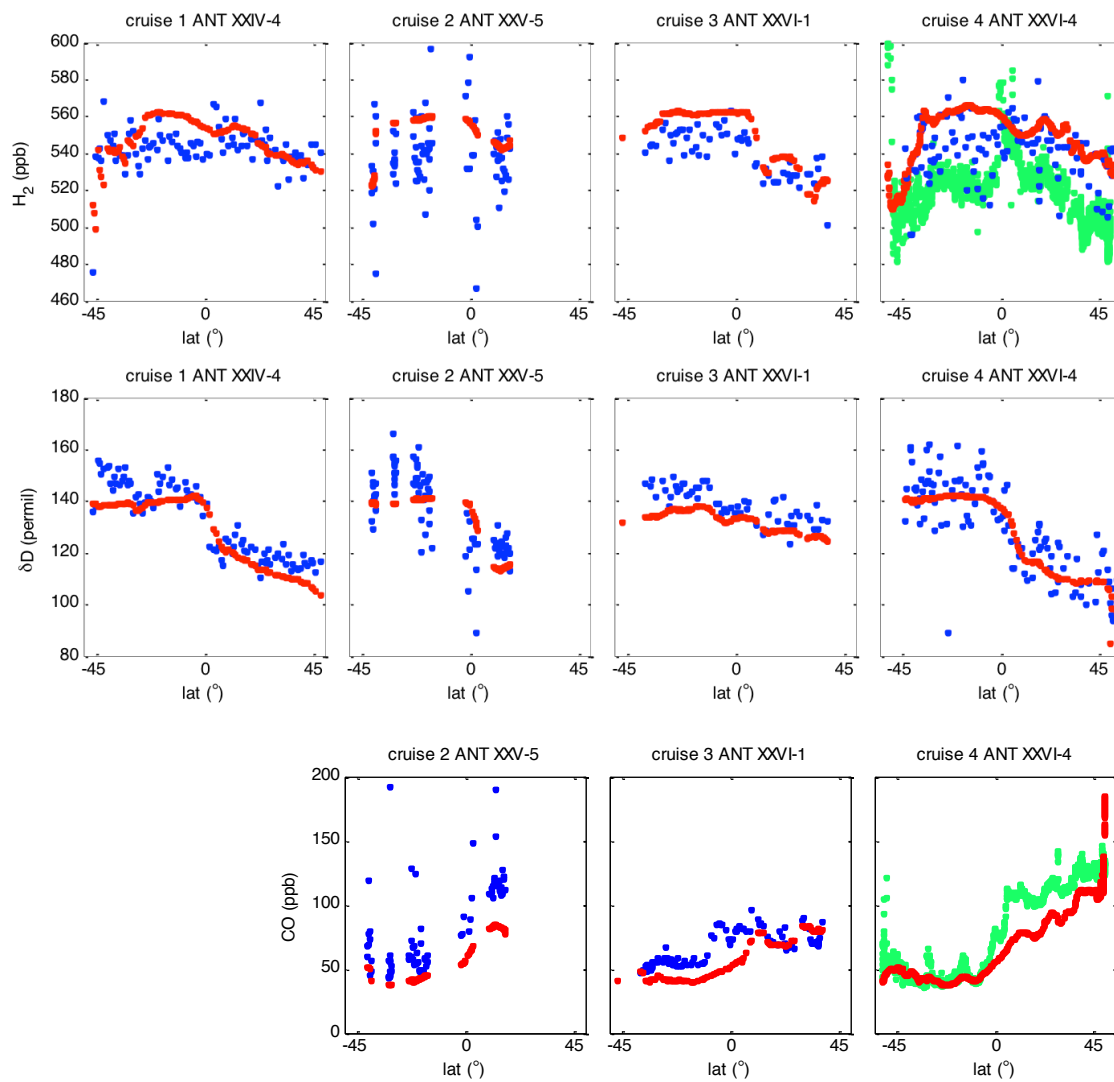


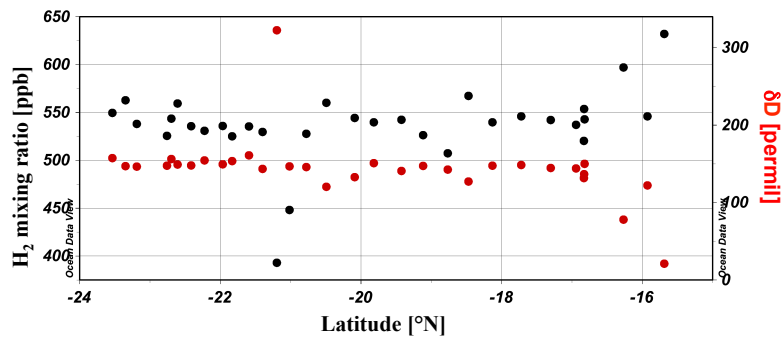
Figure 5: Comparison of measurement results of  $H_2$  and CO mole fractions and  $\delta D$  with TM5 model results (given in red). Data are shown against latitude. The blue markers show results of flask samples, the green markers represent the continuous in-situ measurements (performed with the peak performer instrument on-board). CO has not been analysed in the flasks sampled during the last cruise. The model data were interpolated at the place and time of sampling or measurements.

2

3

1

a)



b)

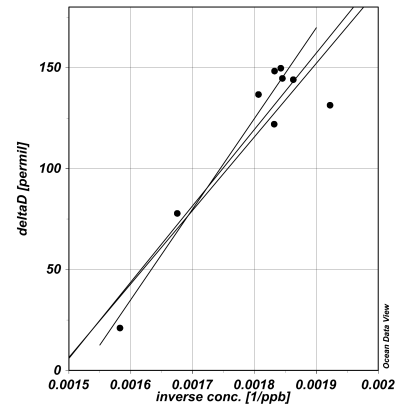


Figure 6: a) H<sub>2</sub> mole fraction [ppb] (black) and δD [‰] (red) along the ANT-XXV/5 high-resolution transect 24° S–15° S; b) Keeling plot of the samples along the high-resolution transect north of 18° S. The three trend lines indicate the range of the Keeling plot analysis that was applied to determine the source signature.

2

3

4

5

6

7

8

9

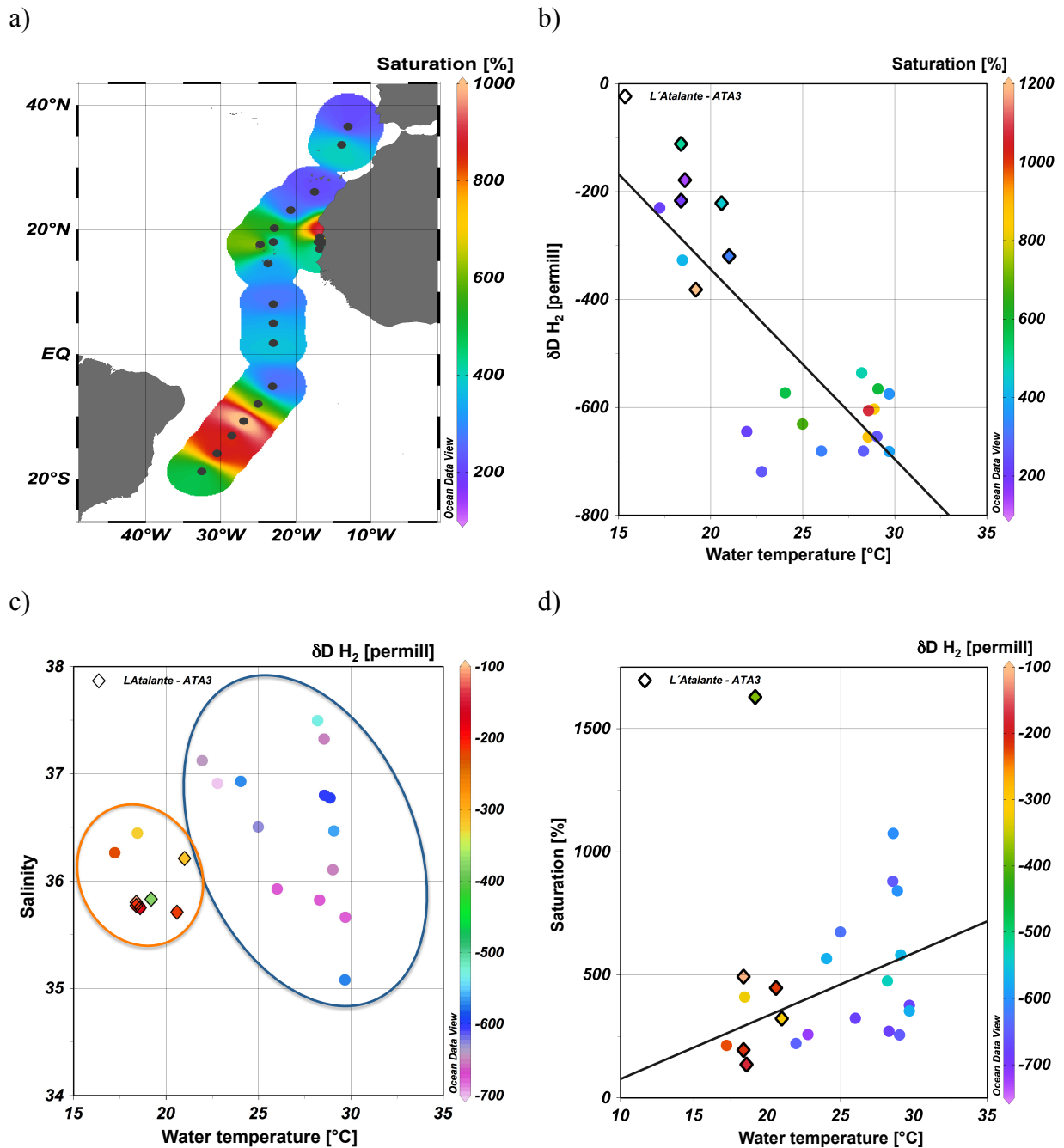


Figure 7:

a) H<sub>2</sub> saturation in the surface water (color coded) along the RV *Polarstern* cruise track of ANT-XXVI/4 and the RV *L'Atalante* cruise ATA-3, with maxima around the Cape Verde islands and 10–15° S, Note: each sample is represented by a single dot.

b) Comparing the δD (H<sub>2</sub>) at different water temperatures, the respective H<sub>2</sub> saturations are color coded, sample dots marked with a diamond belong to the RV *L'Atalante* cruise, sample dots without to the ANT-XXVI/4 cruise;  $y = -35.2x + 360.9$ ,  $R^2 = 0.66$ ,  $n = 22$

c) Distribution of δD (H<sub>2</sub>) (color coded) in correlation between water temperature and salinity

d) Correlation between water temperature and H<sub>2</sub> saturation, the δD (H<sub>2</sub>) is color-coded, the exceptional high saturation has been excluded from the correlation calculation,  $y = 0.26x - 2.79$ ,  $R^2 = 0.22$ ,  $n = 21$

1

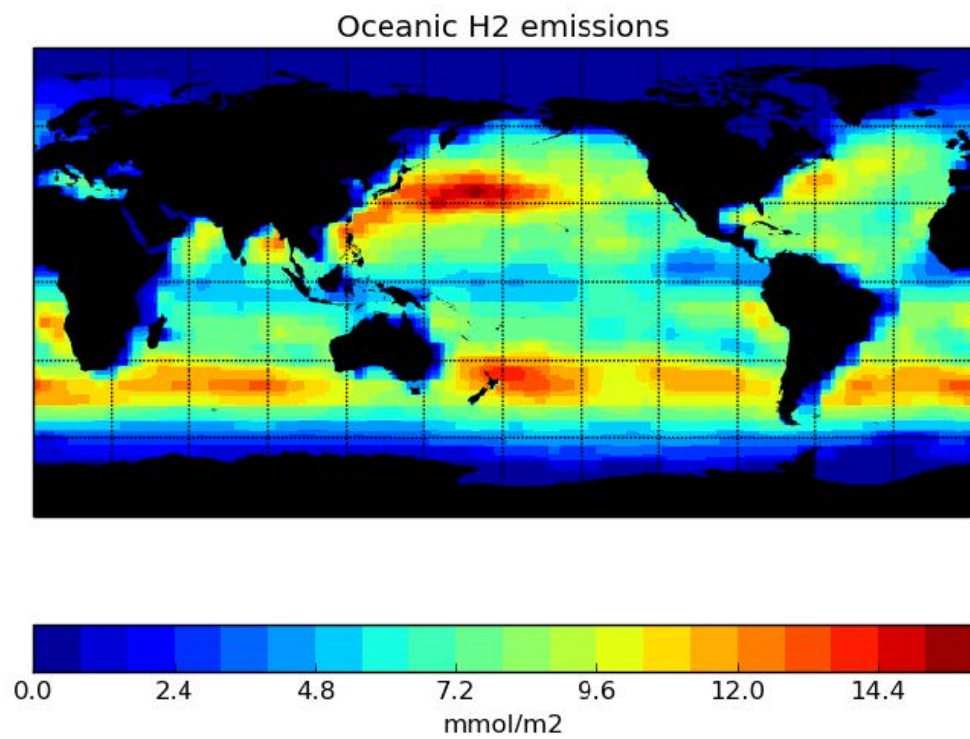


Figure 8: Oceanic H<sub>2</sub> emissions used in the TM5 model simulations ( $\text{mmol m}^{-2} \text{a}^{-1}$ , based on the distribution provided by the project GEMS (Global and regional Earth-system (Atmosphere) Monitoring using Satellite and in-situ data) and scaled to a total oceanic source of  $5 \text{ Tg a}^{-1}$  (Pieterse et al. (2013))

2